Max-Planck-Institute Für Astronomie & Indian Institute of Technology Indore

Extragalactic jets on all scales - launching, propagation, termination

Flux variability from ejecta in structured relativistic jets with large-scale magnetic fields

Fichet de Clairfontaine Gaëtan with Zakaria Meliani, Andreas Zech and Olivier Hervet
Laboratoire Univers et Théories - Observatoire de Paris

Context

« RADIO LOUD » AGN :

- The luminosity can reach extremely high values $L_{\text{tot}} \sim 10^{47}$ erg · s^{-1};
- Non thermal emission, extended from radio up to very high energy gamma rays;
- Presence of stationary emission zones in the jet (knots).

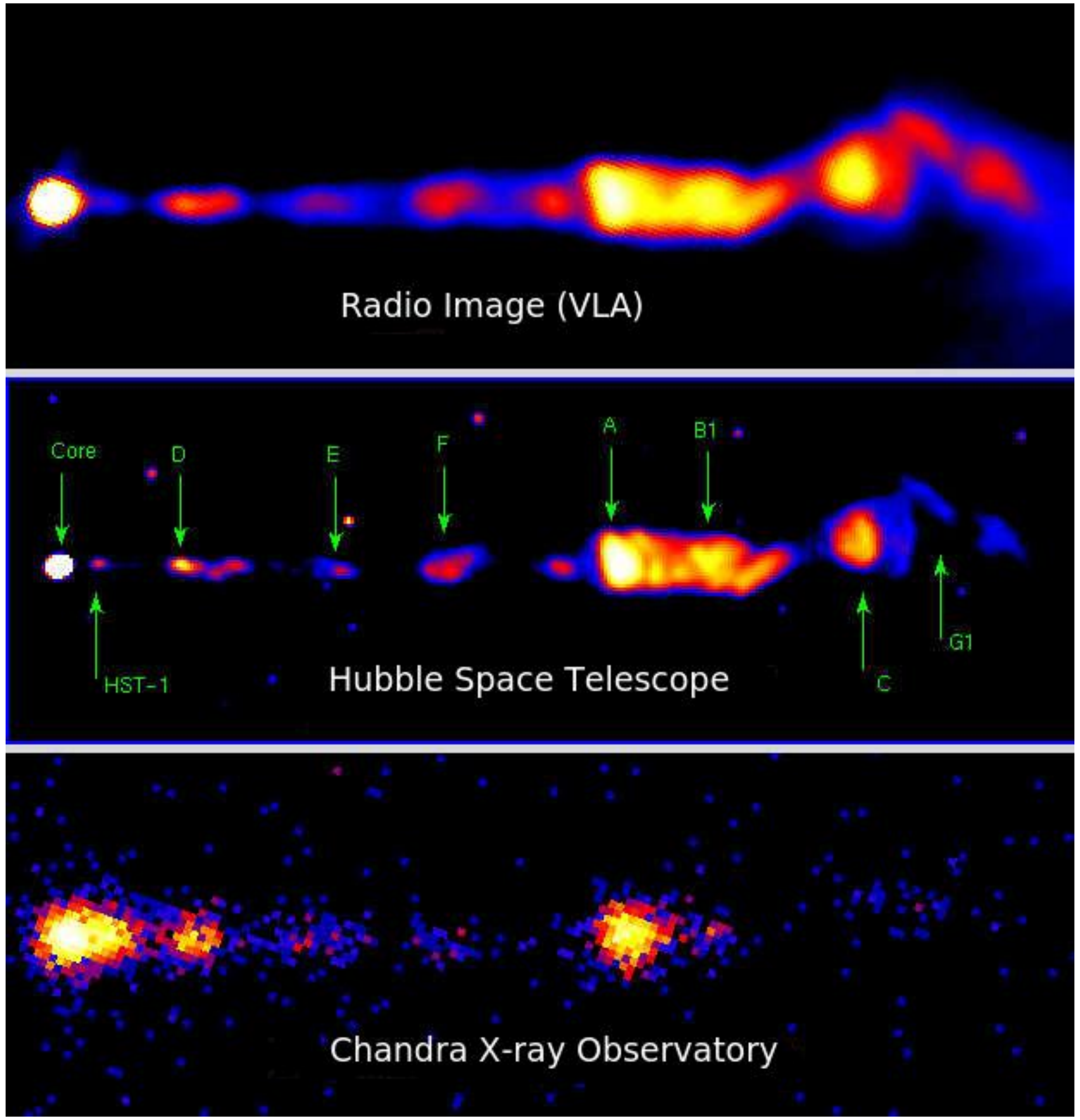

Panel of optical, radio observation maps (Perlman et al. 1999) and X-ray maps (Marshall et al. 2002) of the M87 jet.

Context

« RADIO LOUD » AGN :

- The luminosity can reach extremely high values $L_{\mathrm{tot}} \sim 10^{47}$ erg · s^{-1};
- Non thermal emission, extended from radio up to very high energy gamma rays;
- Presence of stationary emission zones in the jet (knots).

ELECTRON ACCELERATION AT SHOCKS :

- Flux variability observed at various wavelengths (sometimes simultaneously);
- Observation of emission zones moving at ultra-relativistic speeds;

‣ **Fermi I acceleration type on shocks.**

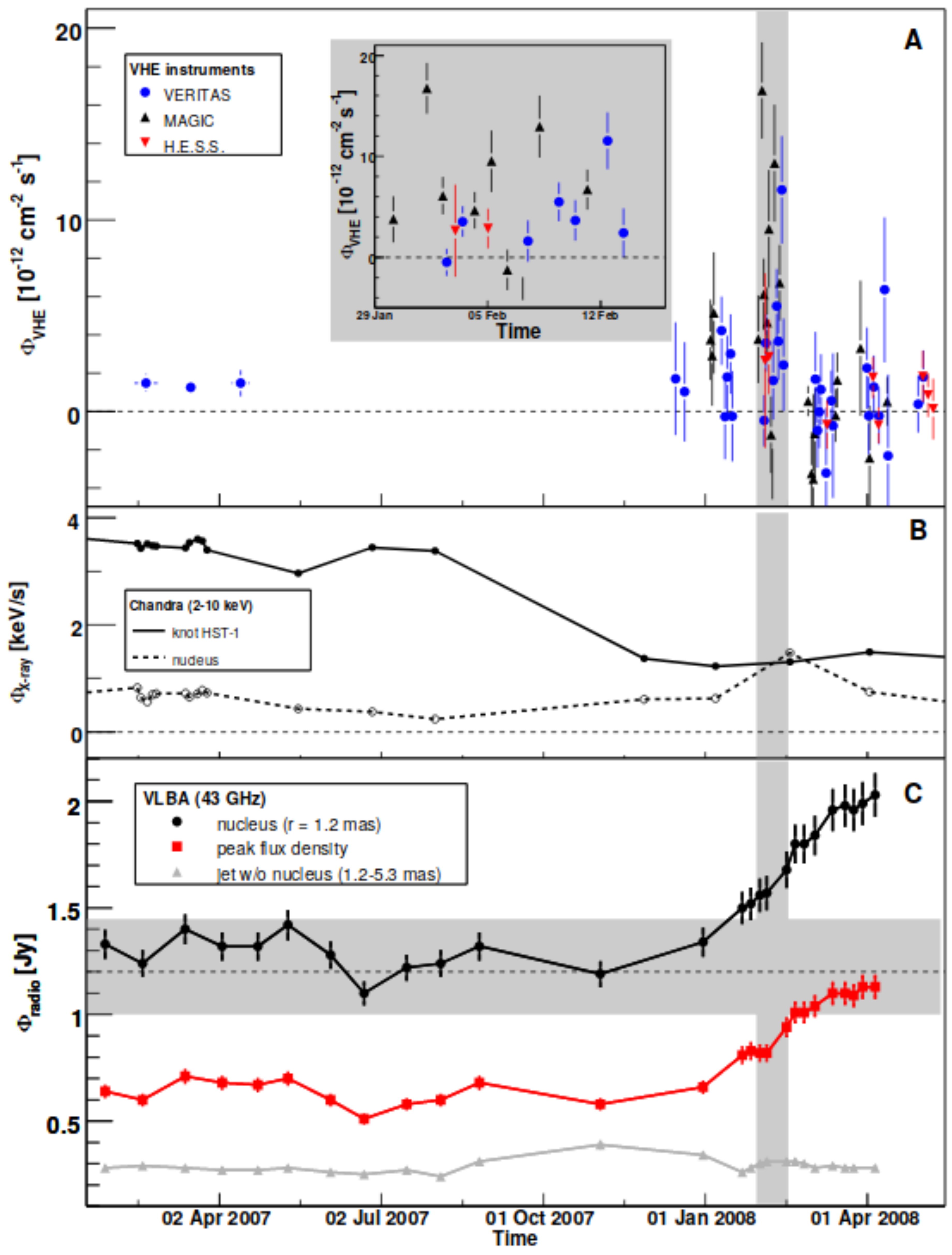

M87 - Acciari et al. 2009.

Context

« RADIO LOUD » AGN :

- The luminosity can reach extremely high values $L_{\text{tot}} \sim 10^{47}$ erg · s^{-1};
- Non thermal emission, extended from radio up to very high energy gamma rays;
- Presence of stationary emission zones in the jet (knots).

ELECTRON ACCELERATION AT SHOCKS :

- Flux variability observed at various wavelengths (sometimes simultaneously);
- Observation of emission zones moving at ultra-relativistic speeds;
- **Fermi I acceleration type on shocks.**

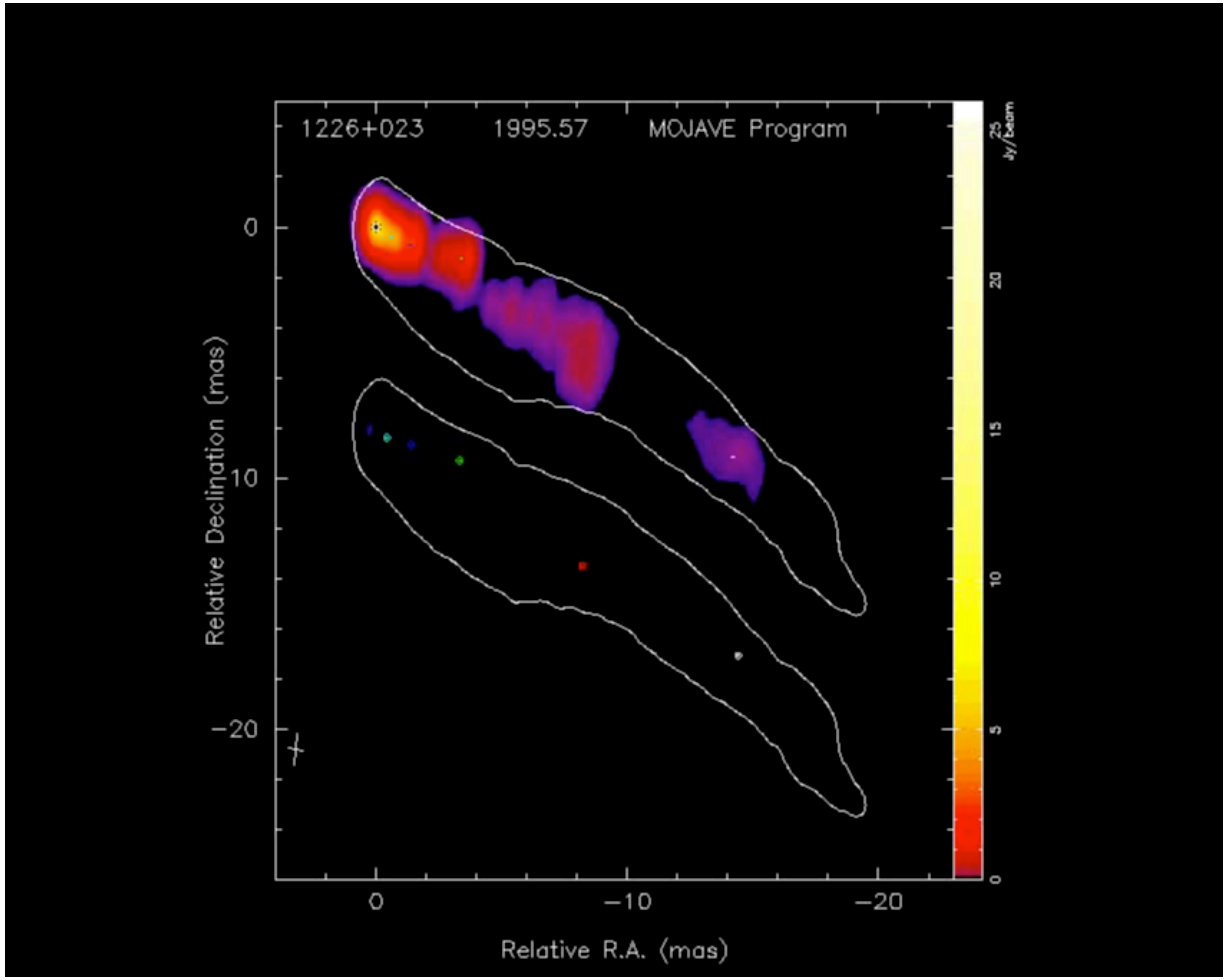

MOJAVE PROGRAM - OVRO 15 GHz (Lister et al. 2018)

Context

« RADIO LOUD » AGN :

- The luminosity can reach extremely high values $L_{\text{tot}} \sim 10^{47}$ erg · s^{-1};
- Non thermal emission, extended from radio up to very high energy gamma rays;
- Presence of stationary emission zones in the jet (knots).

ELECTRON ACCELERATION AT SHOCKS :

- Flux variability observed at various wavelengths (sometimes simultaneously);
- Observation of emission zones moving at ultra-relativistic speeds;

‣ **Fermi I acceleration type on shocks.**

QUESTIONS :

- Can we reproduce observed jet characteristics (standing / moving knots) ?
- Origin and localization of variability ? Can it be explained by the interaction of the jet (recollimation shocks) with a moving shock zone ?

➡ Complete model: SMHRD + radiative processes !

SRMHD

MPI-AMRVAC (KEPPENS ET AL. 2012) :

- Solving the equations of the relativistic MHD in each cell within an adaptive mesh;
- Four zones simulated : each with a set of initial conditions;
- Ejecta : spherical zone insert at the base of the inner jet (over pressure / denser zone).

Radiative processes

POST PROCESSING :

- Injection following a power-law between two cut-off values;
- K depends on the density and thermal energy medium, as well as $\gamma_{\mathrm{e,min}}$ (Gomez et al. 1995).
- Our model takes into account Doppler relativistic effects with the observation angle θ_{obs}.

SRMHD

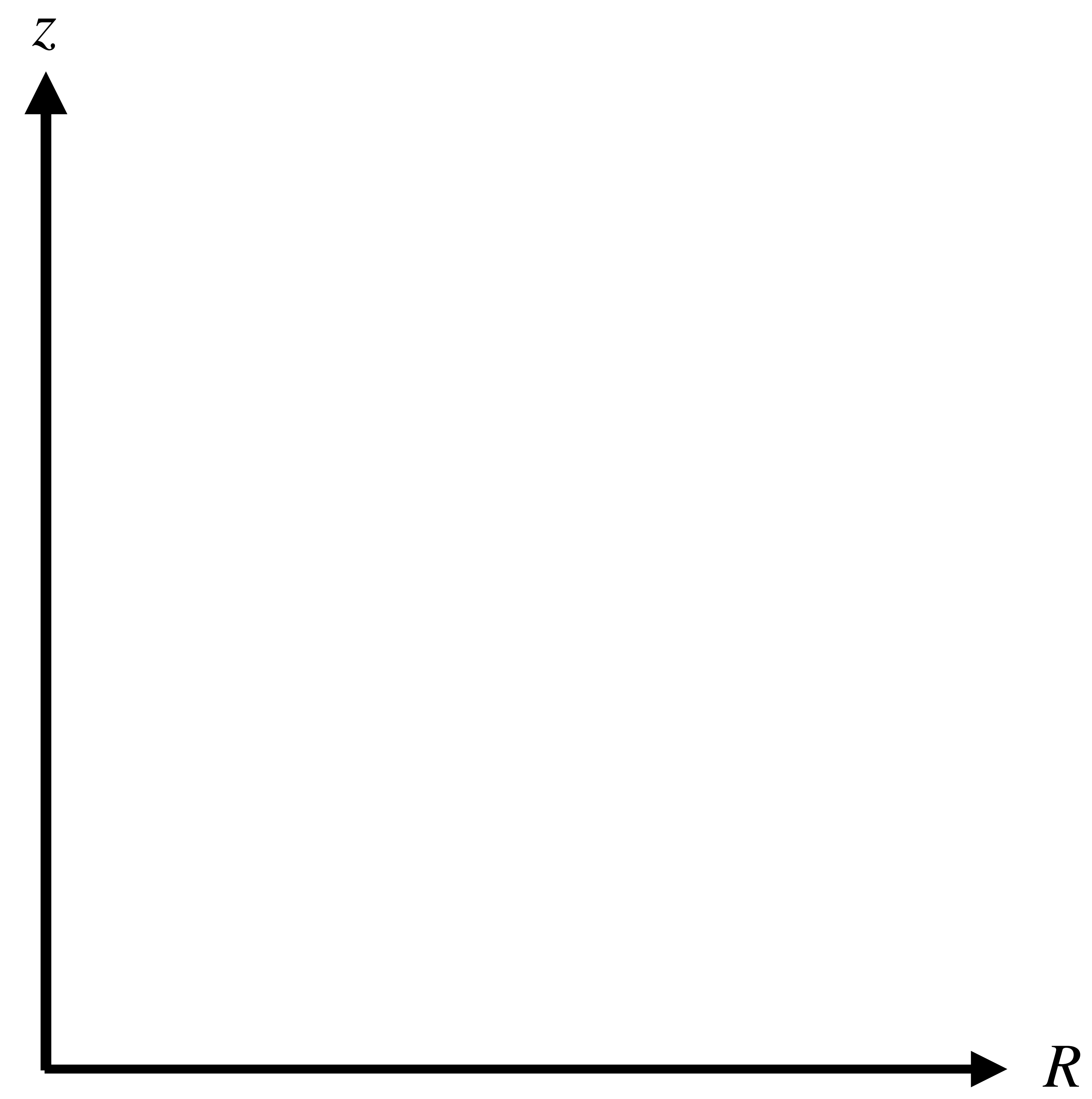

MPI-AMRVAC (KEPPENS ET AL. 2012) :

- Solving the equations of the relativistic MHD in each cell within an adaptive mesh;
- Four zones simulated : each with a set of initial conditions;
- Ejecta : spherical zone insert at the base of the inner jet (over pressure / denser zone).

Radiative processes

POST PROCESSING :

- Injection following a power-law between two cut-off values;
- K depends on the density and thermal energy medium, as well as $\gamma_{\mathrm{e,min}}$ (Gomez et al. 1995).
- Our model takes into account Doppler relativistic effects with the observation angle θ_{obs}.

SRMHD

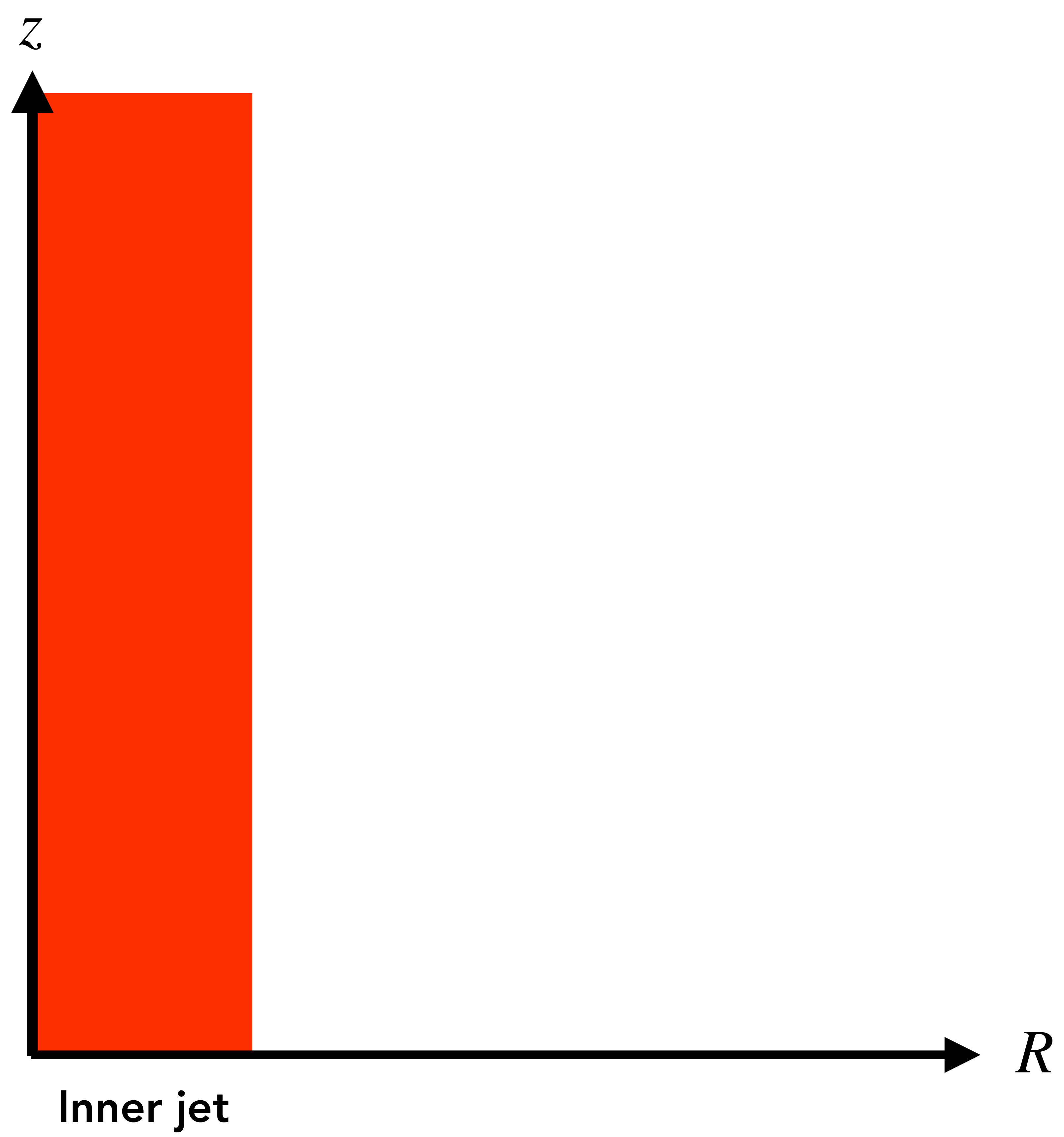

MPI-AMRVAC (KEPPENS ET AL. 2012) :

- Solving the equations of the relativistic MHD in each cell within an adaptive mesh;
- Four zones simulated : each with a set of initial conditions;
- Ejecta : spherical zone insert at the base of the inner jet (over pressure / denser zone).

Radiative processes

POST PROCESSING :

- Injection following a power-law between two cut-off values;
- K depends on the density and thermal energy medium, as well as $\gamma_{e,min}$ (Gomez et al. 1995).
- Our model takes into account Doppler relativistic effects with the observation angle θ_{obs}.

SRMHD

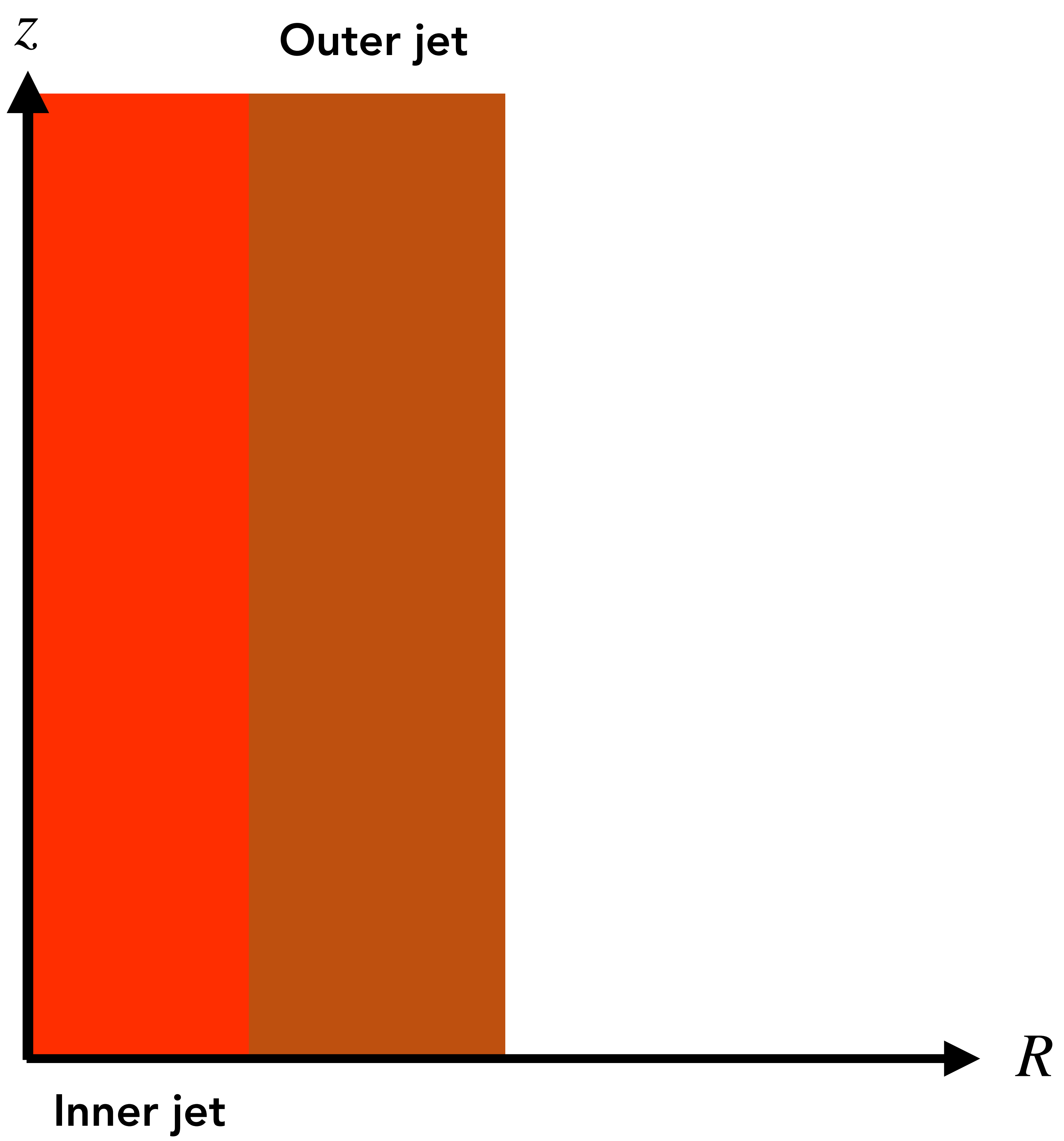

MPI-AMRVAC (KEPPENS ET AL. 2012) :

- Solving the equations of the relativistic MHD in each cell within an adaptive mesh;
- Four zones simulated : each with a set of initial conditions;
- Ejecta : spherical zone insert at the base of the inner jet (over pressure / denser zone).

Radiative processes

POST PROCESSING :

- Injection following a power-law between two cut-off values;
- K depends on the density and thermal energy medium, as well as $\gamma_{\mathrm{e,min}}$ (Gomez et al. 1995).
- Our model takes into account Doppler relativistic effects with the observation angle θ_{obs}.

SRMHD

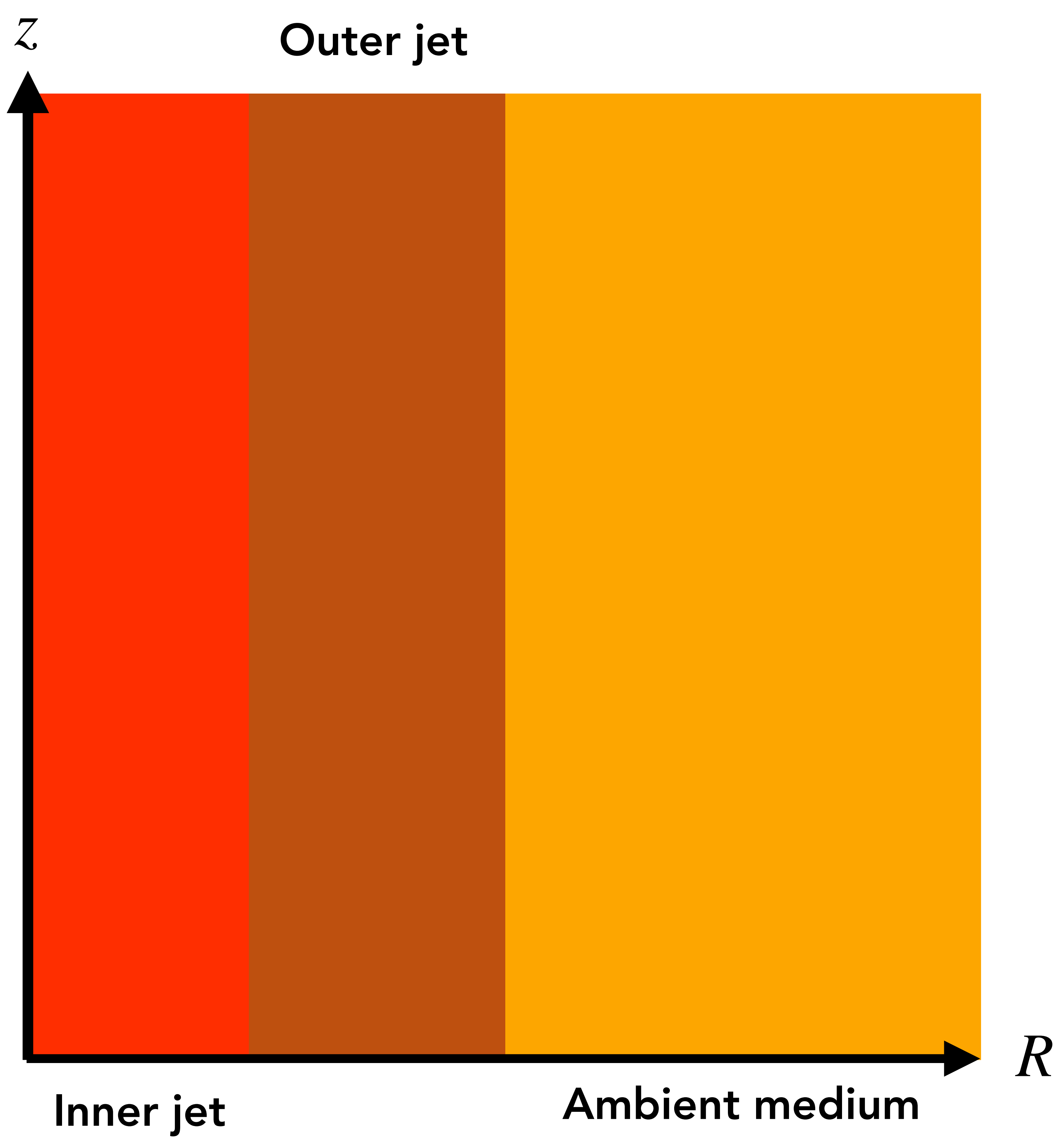

MPI-AMRVAC (KEPPENS ET AL. 2012) :

- Solving the equations of the relativistic MHD in each cell within an adaptive mesh;
- Four zones simulated : each with a set of initial conditions;
- Ejecta : spherical zone insert at the base of the inner jet (over pressure / denser zone).

Radiative processes

POST PROCESSING :

- Injection following a power-law between two cut-off values;
- K depends on the density and thermal energy medium, as well as $\gamma_{e,min}$ (Gomez et al. 1995).
- Our model takes into account Doppler relativistic effects with the observation angle θ_{obs}.

SRMHD

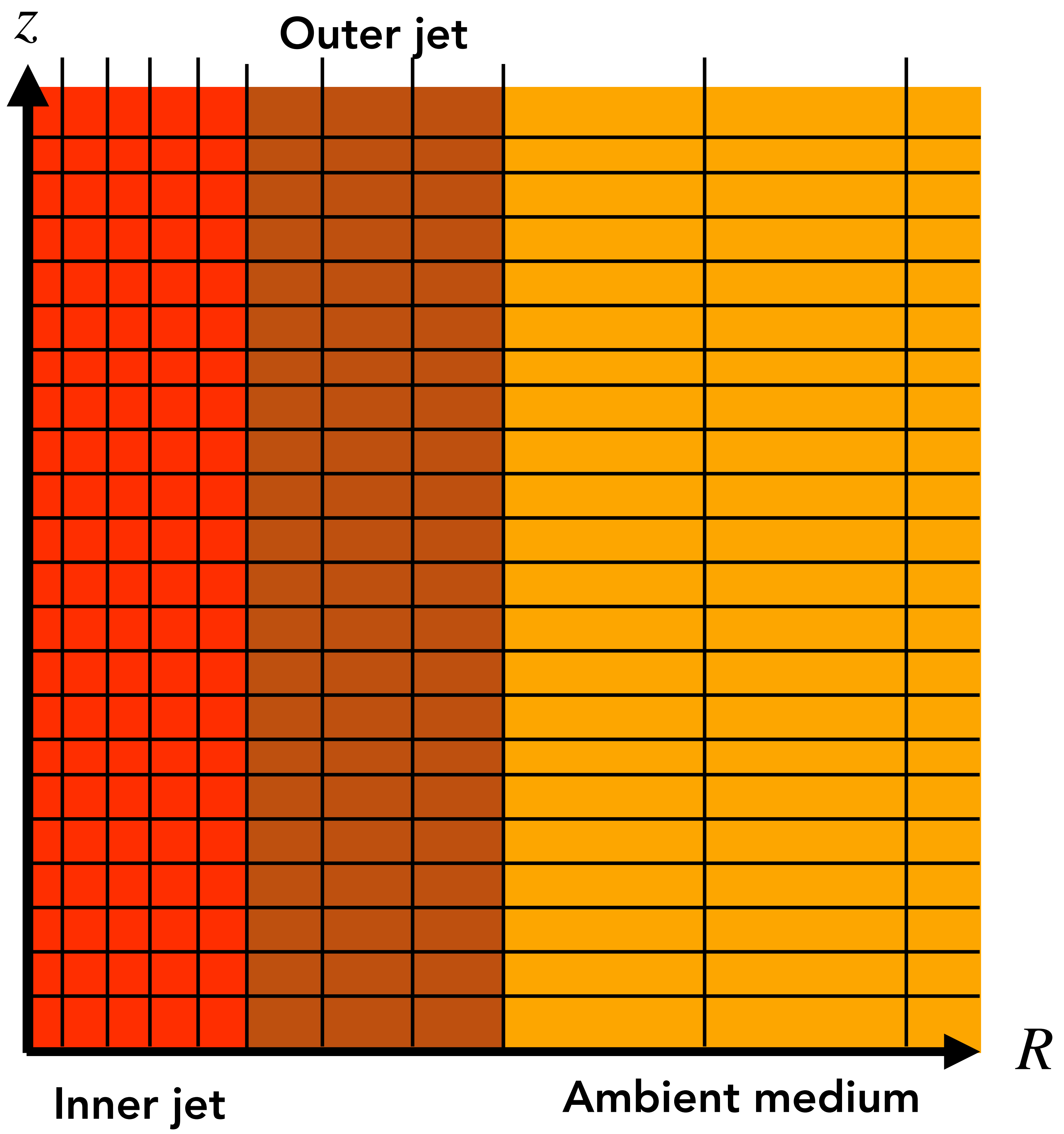

MPI-AMRVAC (KEPPENS ET AL. 2012) :

- Solving the equations of the relativistic MHD in each cell within an adaptive mesh;
- Four zones simulated : each with a set of initial conditions;
- Ejecta : spherical zone insert at the base of the inner jet (over pressure / denser zone).

Radiative processes

POST PROCESSING :

- Injection following a power-law between two cut-off values;
- K depends on the density and thermal energy medium, as well as $\gamma_{\mathrm{e,min}}$ (Gomez et al. 1995).
- Our model takes into account Doppler relativistic effects with the observation angle θ_{obs}.

SRMHD

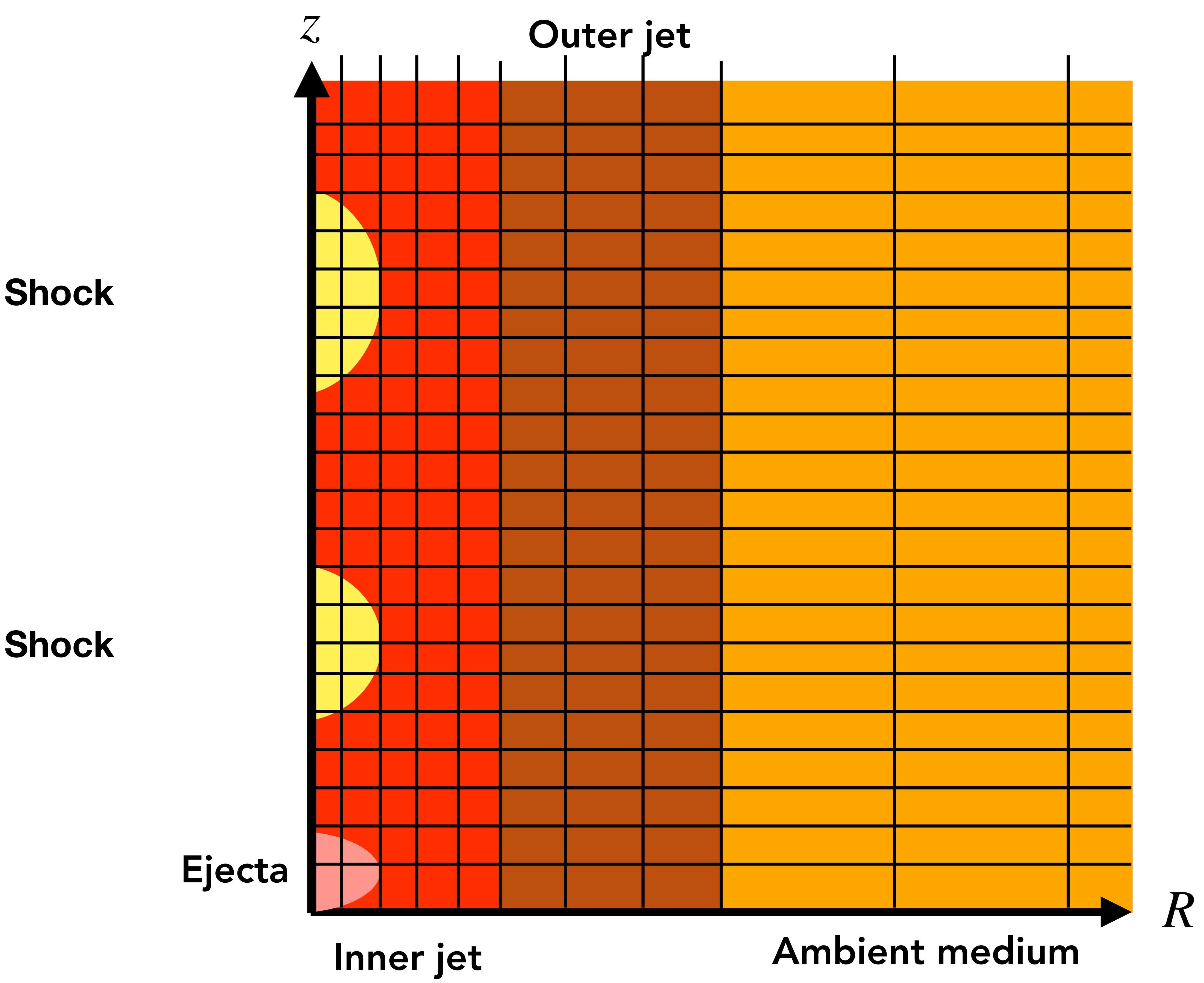

MPI-AMRVAC (KEPPENS ET AL. 2012) :

- Solving the equations of the relativistic MHD in each cell within an adaptive mesh;
- Four zones simulated : each with a set of initial conditions;
- Ejecta : spherical zone insert at the base of the inner jet (over pressure / denser zone).

Radiative processes

POST PROCESSING :

- Injection following a power-law between two cut-off values;
- K depends on the density and thermal energy medium, as well as $\gamma_{e,min}$ (Gomez et al. 1995).
- Our model takes into account Doppler relativistic effects with the observation angle θ_{obs}.

SRMHD

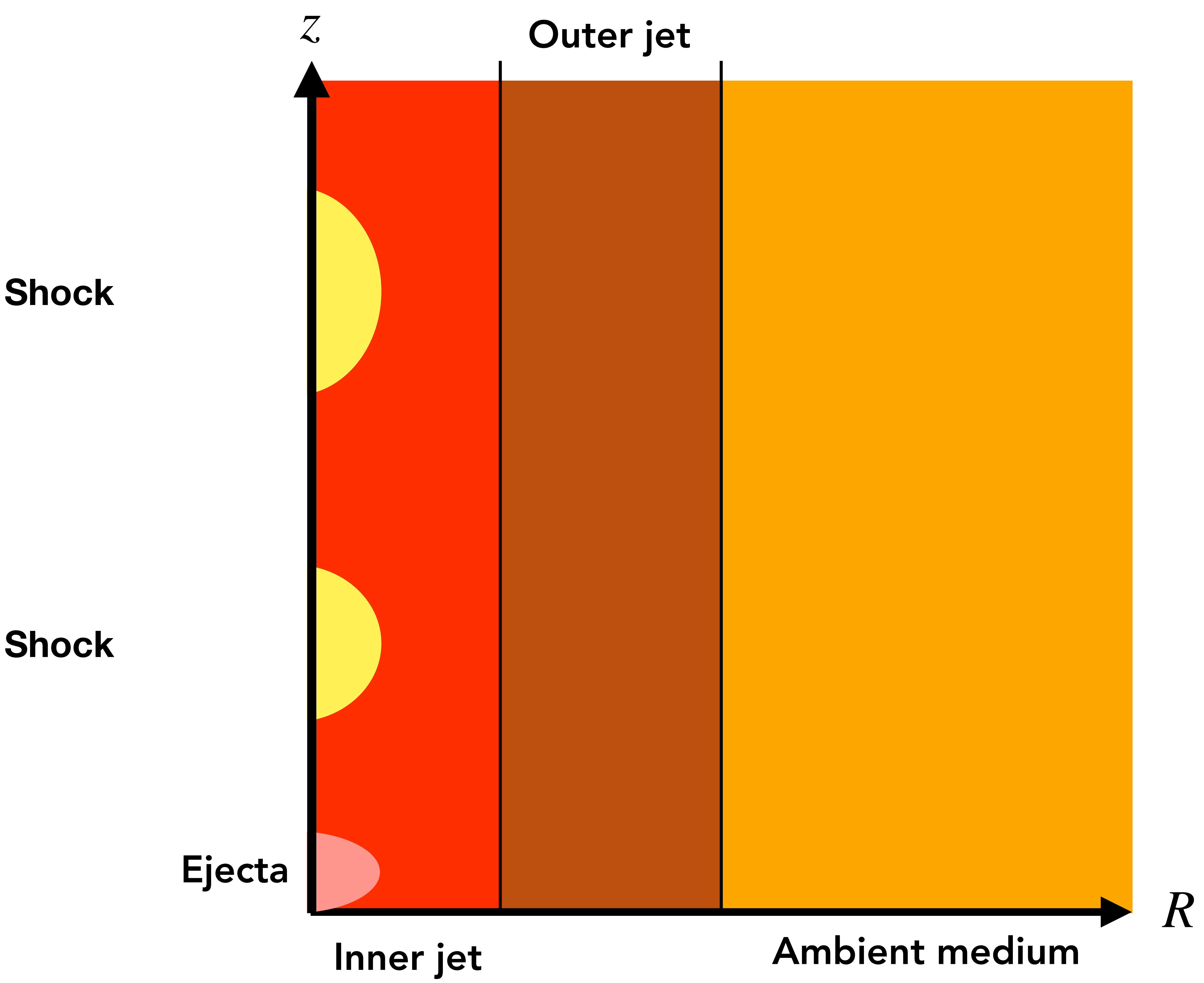

MPI-AMRVAC (KEPPENS ET AL. 2012) :

- Solving the equations of the relativistic MHD in each cell within an adaptive mesh;
- Four zones simulated : each with a set of initial conditions;
- Ejecta : spherical zone insert at the base of the inner jet (over pressure / denser zone).

Radiative processes

POST PROCESSING :

- Injection following a power-law between two cut-off values;
- K depends on the density and thermal energy medium, as well as $\gamma_{e,min}$ (Gomez et al. 1995).
- Our model takes into account Doppler relativistic effects with the observation angle θ_{obs}.

SRMHD

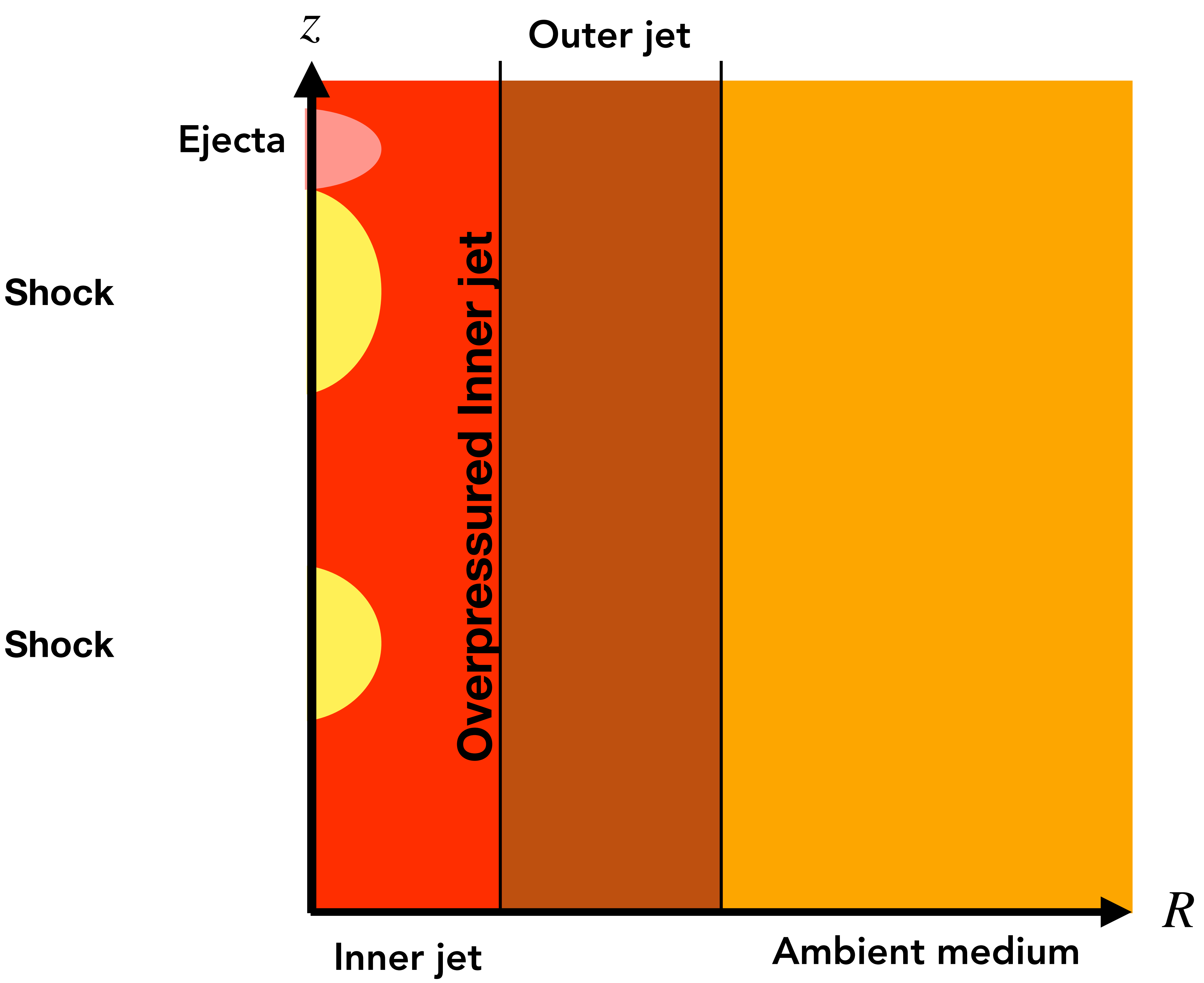

MPI-AMRVAC (KEPPENS ET AL. 2012) :

- Solving the equations of the relativistic MHD in each cell within an adaptive mesh;
- Four zones simulated : each with a set of initial conditions;
- Ejecta : spherical zone insert at the base of the inner jet (over pressure / denser zone).

Radiative processes

POST PROCESSING :

- Injection following a power-law between two cut-off values;
- K depends on the density and thermal energy medium, as well as $\gamma_{\mathrm{e,min}}$ (Gomez et al. 1995).
- Our model takes into account Doppler relativistic effects with the observation angle θ_{obs}.

SRMHD

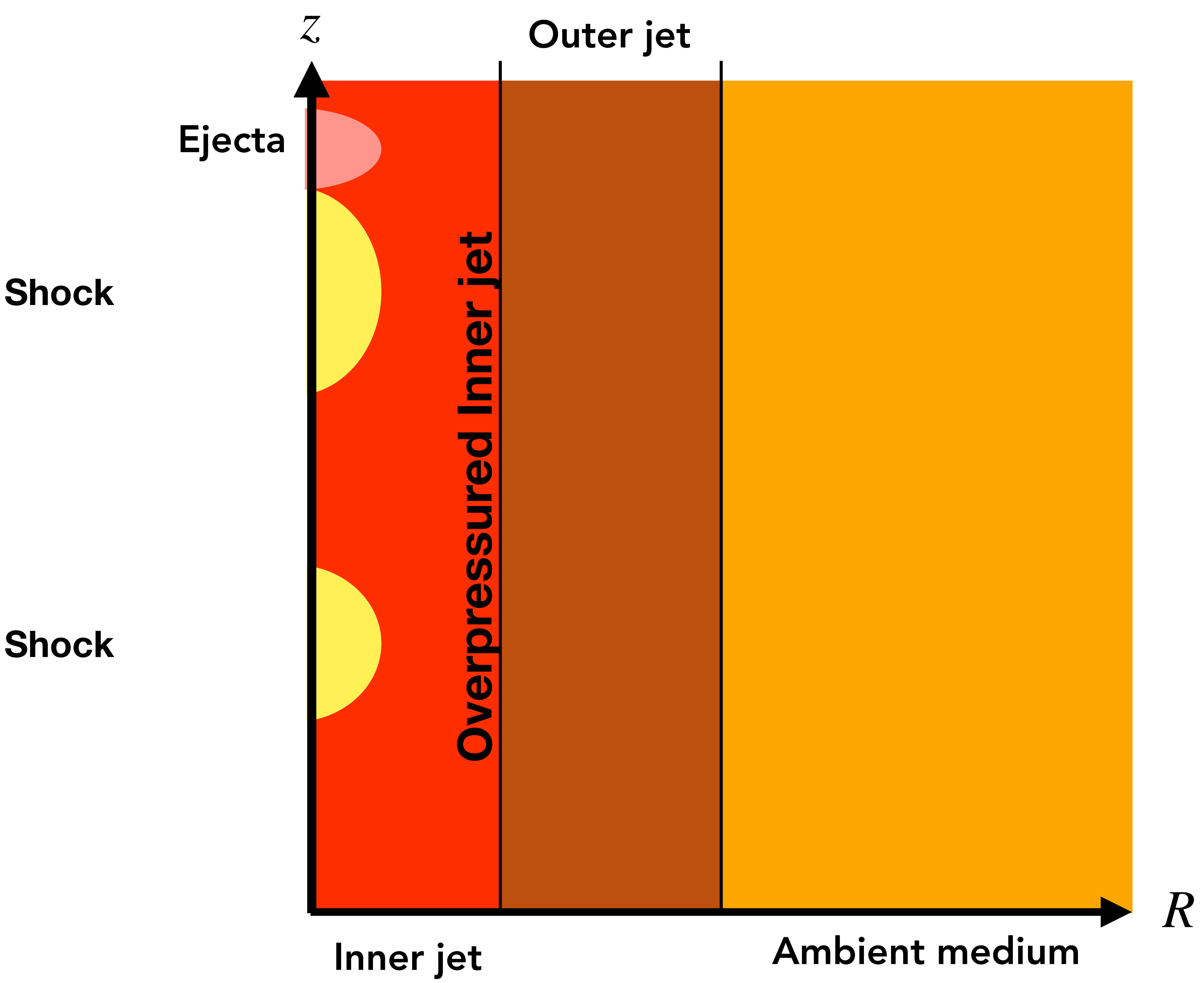

MPI-AMRVAC (KEPPENS ET AL. 2012) :

- Solving the equations of the relativistic MHD in each cell within an adaptive mesh;
- Four zones simulated : each with a set of initial conditions;
- Ejecta : spherical zone insert at the base of the inner jet (over pressure / denser zone).

Radiative processes

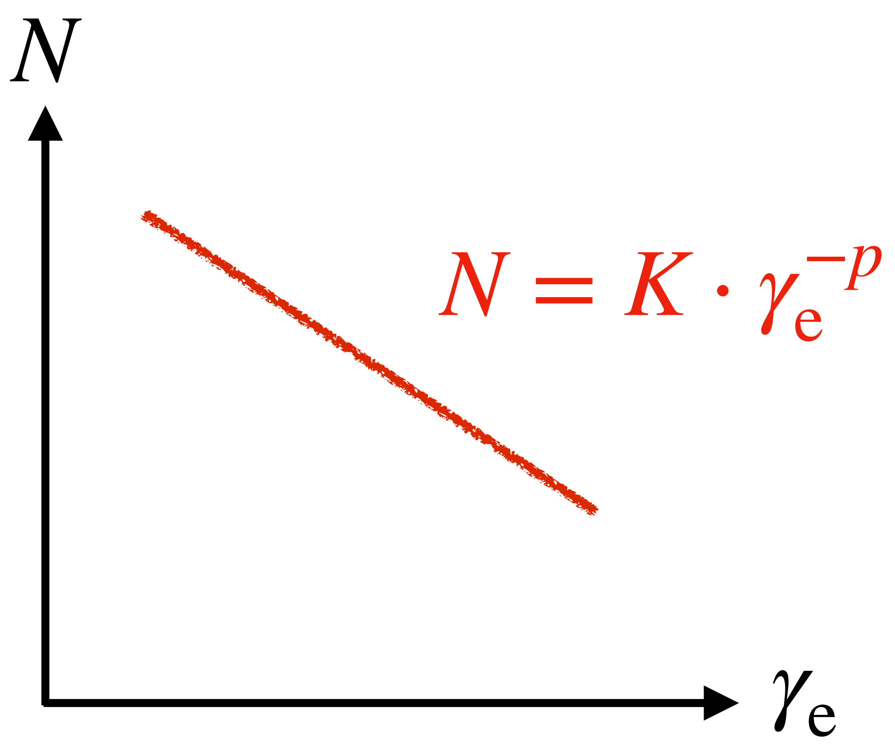

POST PROCESSING :

- Injection following a power-law between two cut-off values;
- K depends on the density and thermal energy medium, as well as $\gamma_{e,min}$ (Gomez et al. 1995).
- Our model takes into account Doppler relativistic effects with the observation angle θ_{obs}.

SRMHD

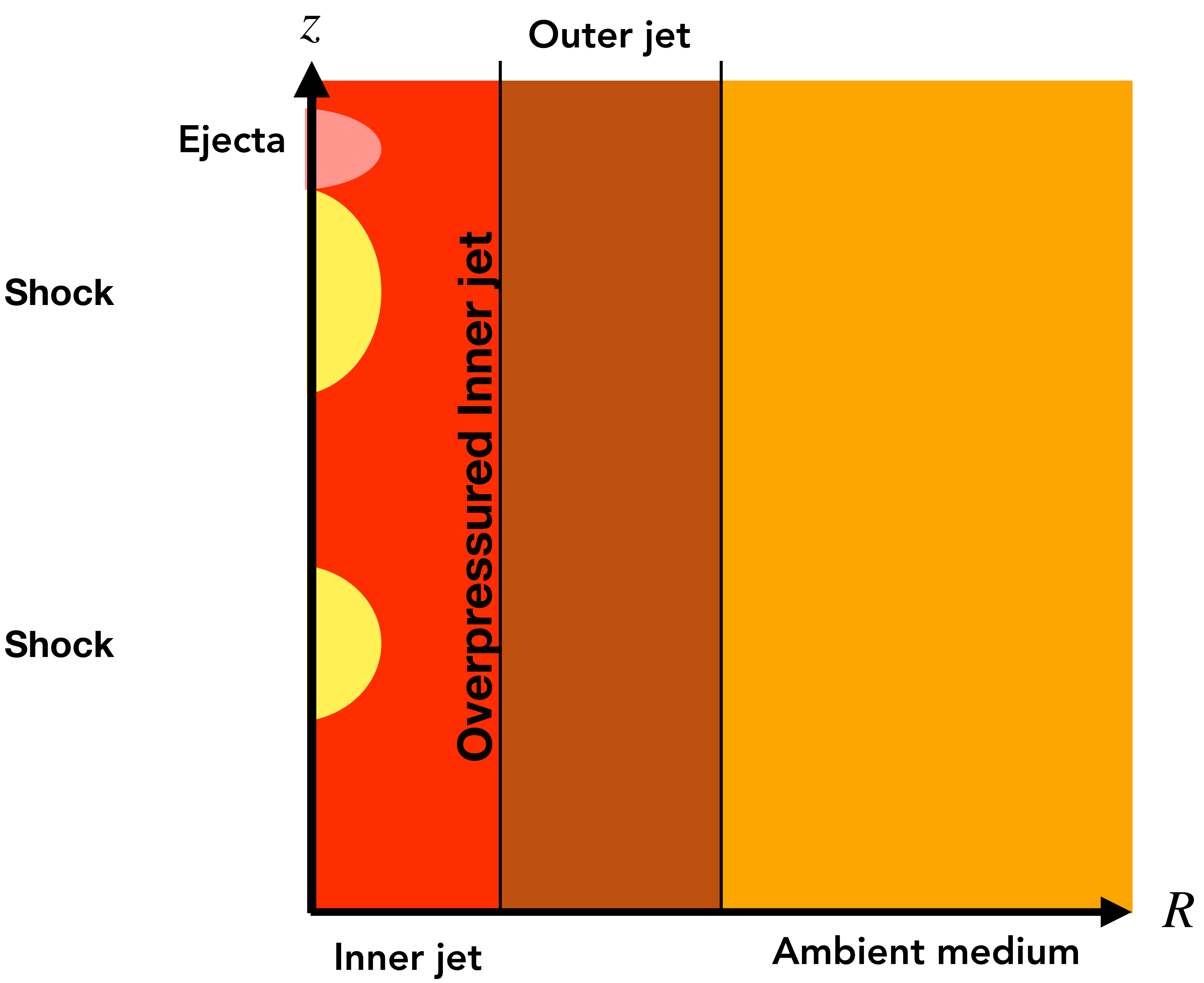

MPI-AMRVAC (KEPPENS ET AL. 2012) :

- Solving the equations of the relativistic MHD in each cell within an adaptive mesh;
- Four zones simulated : each with a set of initial conditions;
- Ejecta : spherical zone insert at the base of the inner jet (over pressure / denser zone).

Radiative processes

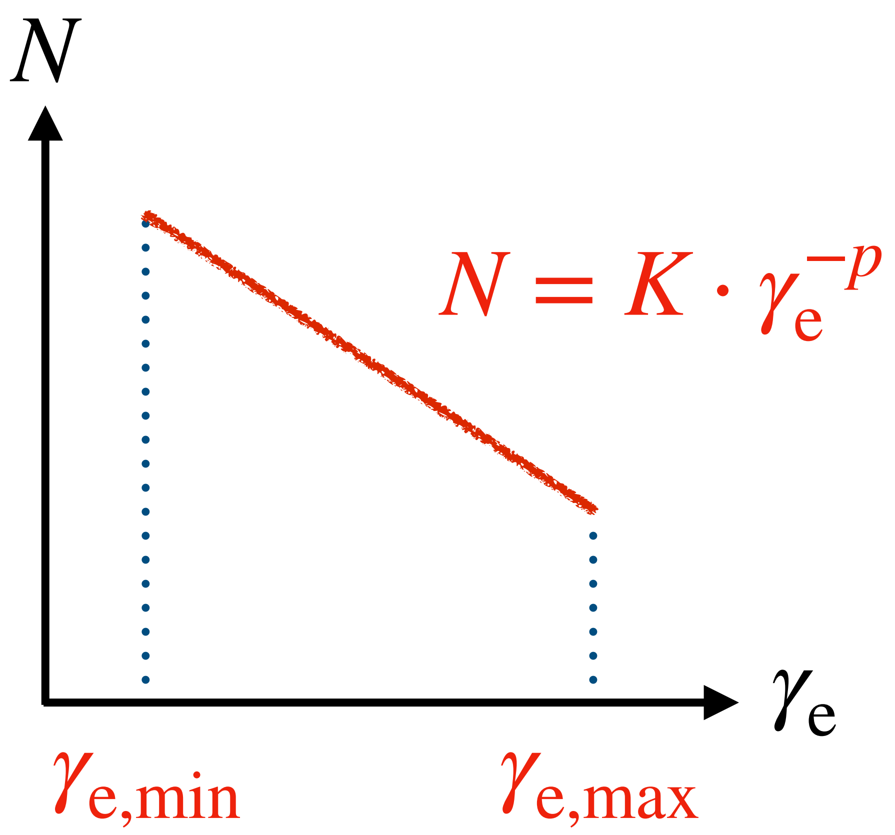

POST PROCESSING :

- Injection following a power-law between two cut-off values;
- K depends on the density and thermal energy medium, as well as $\gamma_{e,min}$ (Gomez et al. 1995).
- Our model takes into account Doppler relativistic effects with the observation angle θ_{obs}.

SRMHD

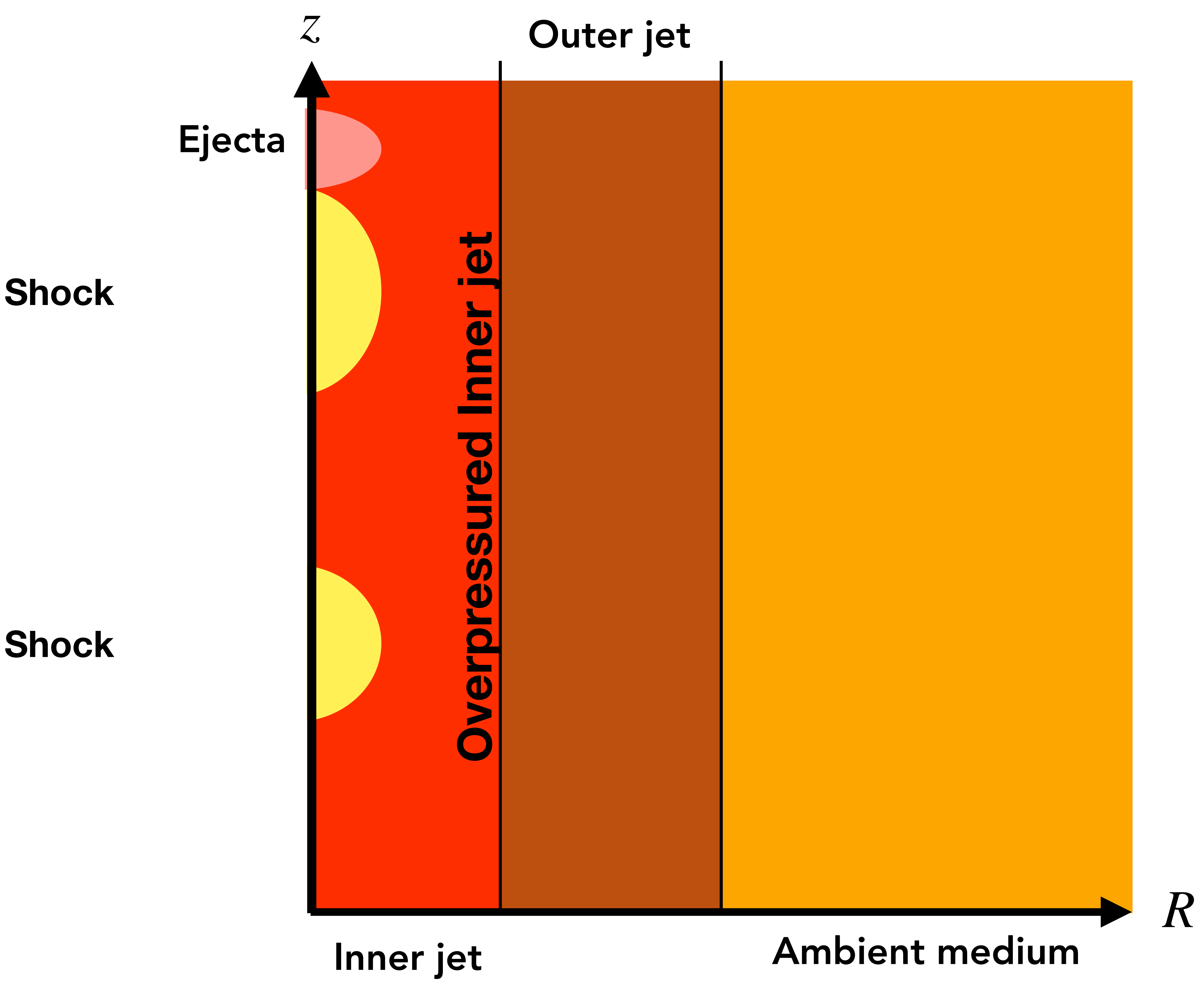

MPI-AMRVAC (KEPPENS ET AL. 2012) :

- Solving the equations of the relativistic MHD in each cell within an adaptive mesh;
- Four zones simulated : each with a set of initial conditions;
- Ejecta : spherical zone insert at the base of the inner jet (over pressure / denser zone).

Radiative processes

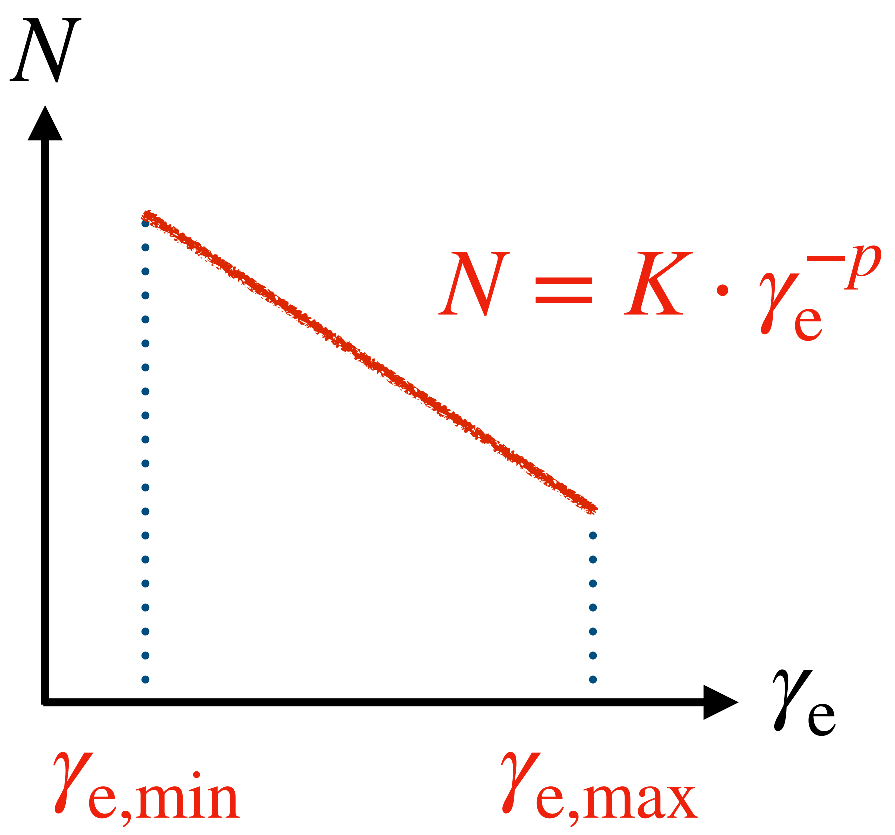

$$K = f(e_{th,e}, C_E, p, n_e)$$

$$e_{th,e} = 0.01 \cdot e_{th}$$

$$n_e = 0.01 \cdot n$$

$$C_E = \gamma_{e,max}/\gamma_{e,min} = 10^3$$

POST PROCESSING :

- Injection following a power-law between two cut-off values;
- K depends on the density and thermal energy medium, as well as $\gamma_{e,min}$ (Gomez et al. 1995).
- Our model takes into account Doppler relativistic effects with the observation angle θ_{obs}.

SRMHD

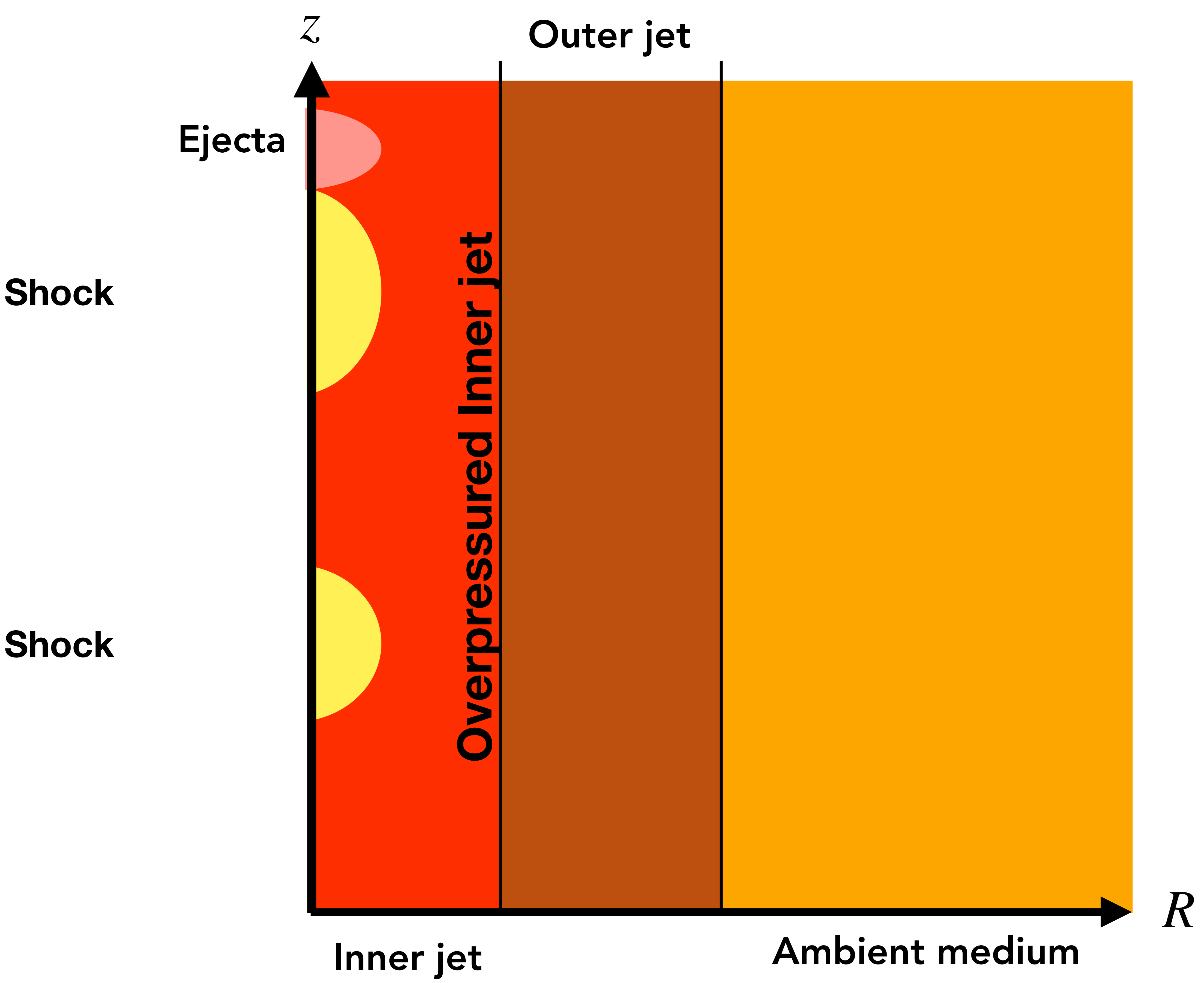

MPI-AMRVAC (KEPPENS ET AL. 2012) :

- Solving the equations of the relativistic MHD in each cell within an adaptive mesh;
- Four zones simulated : each with a set of initial conditions;
- Ejecta : spherical zone insert at the base of the inner jet (over pressure / denser zone).

Radiative processes

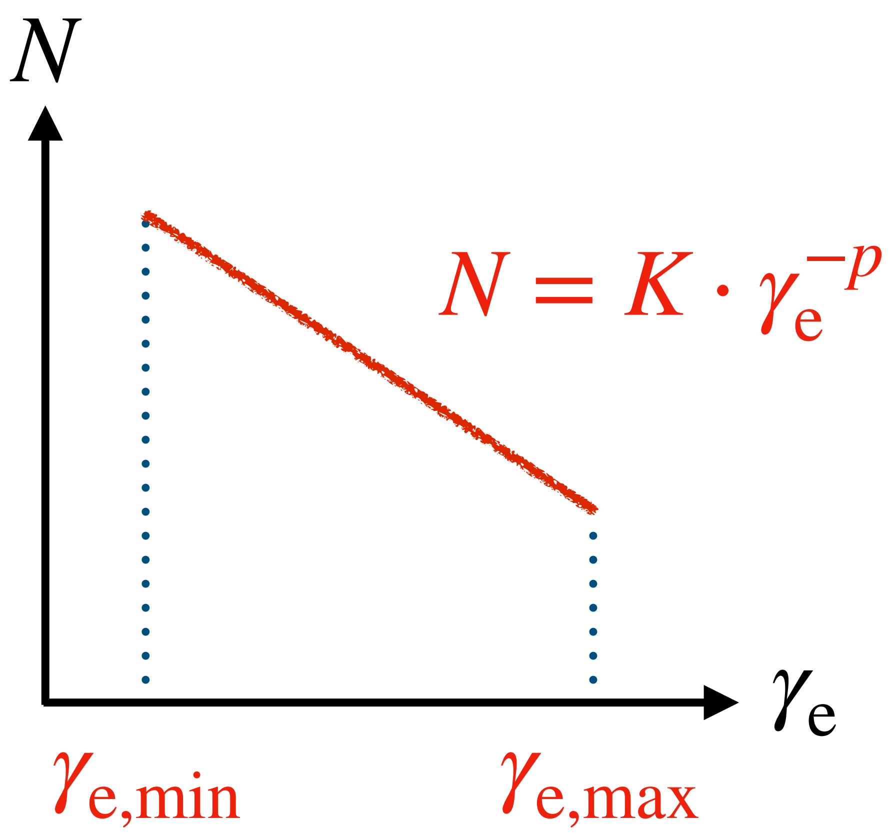

$$K = f(e_{th,e}\,, C_E\,, p\,, n_e\,)$$

$$e_{th,e} = 0.01 \cdot e_{th}$$

$$n_e = 0.01 \cdot n$$

$$C_E = \gamma_{e,max} / \gamma_{e,min} = 10^3$$

→**no radiative losses !**

POST PROCESSING :

- Injection following a power-law between two cut-off values;
- K depends on the density and thermal energy medium, as well as $\gamma_{e,min}$ (Gomez et al. 1995).
- Our model takes into account Doppler relativistic effects with the observation angle θ_{obs}.

SRMHD

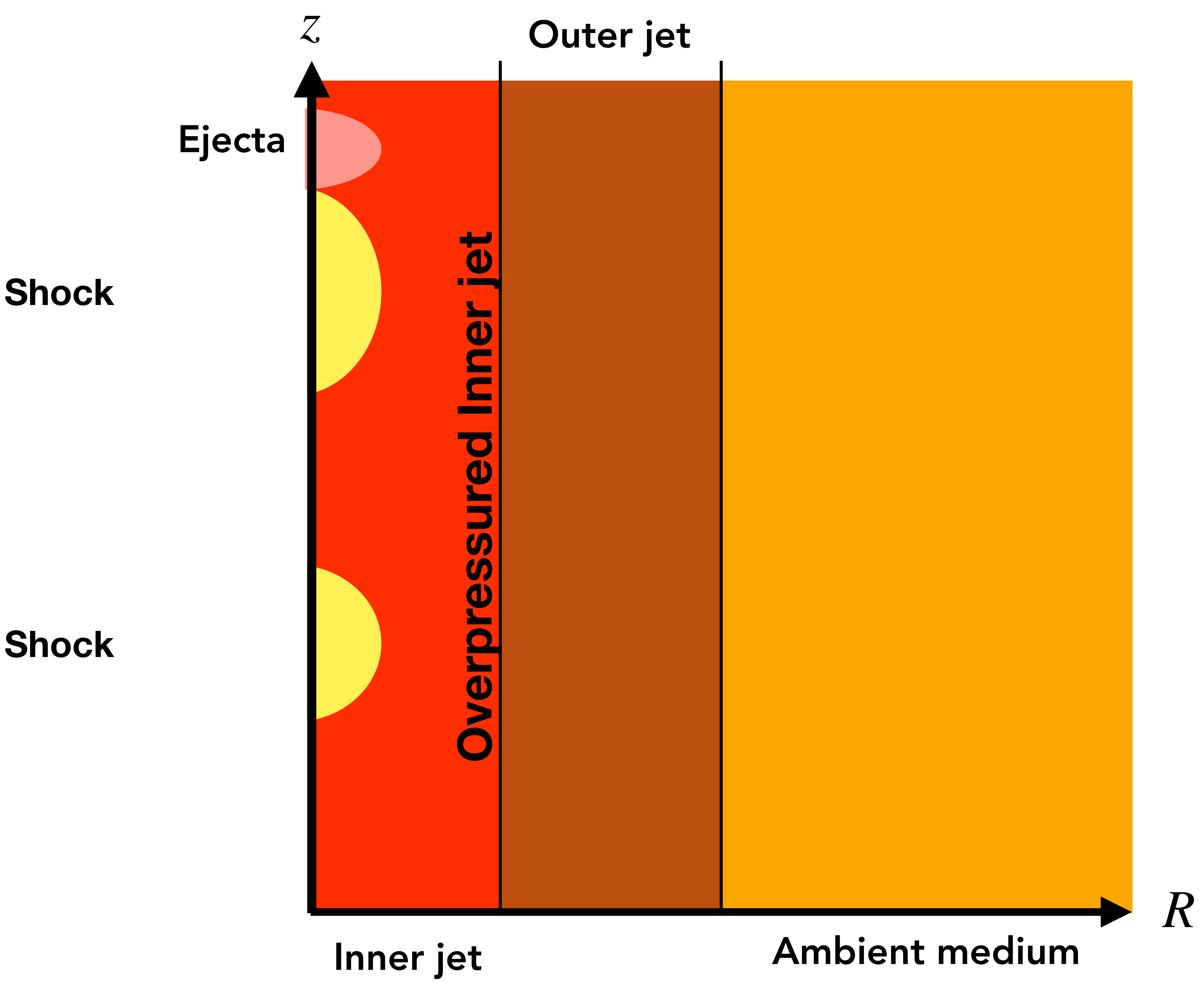

MPI-AMRVAC (KEPPENS ET AL. 2012) :

- Solving the equations of the relativistic MHD in each cell within an adaptive mesh;
- Four zones simulated : each with a set of initial conditions;
- Ejecta : spherical zone insert at the base of the inner jet (over pressure / denser zone).

Radiative processes

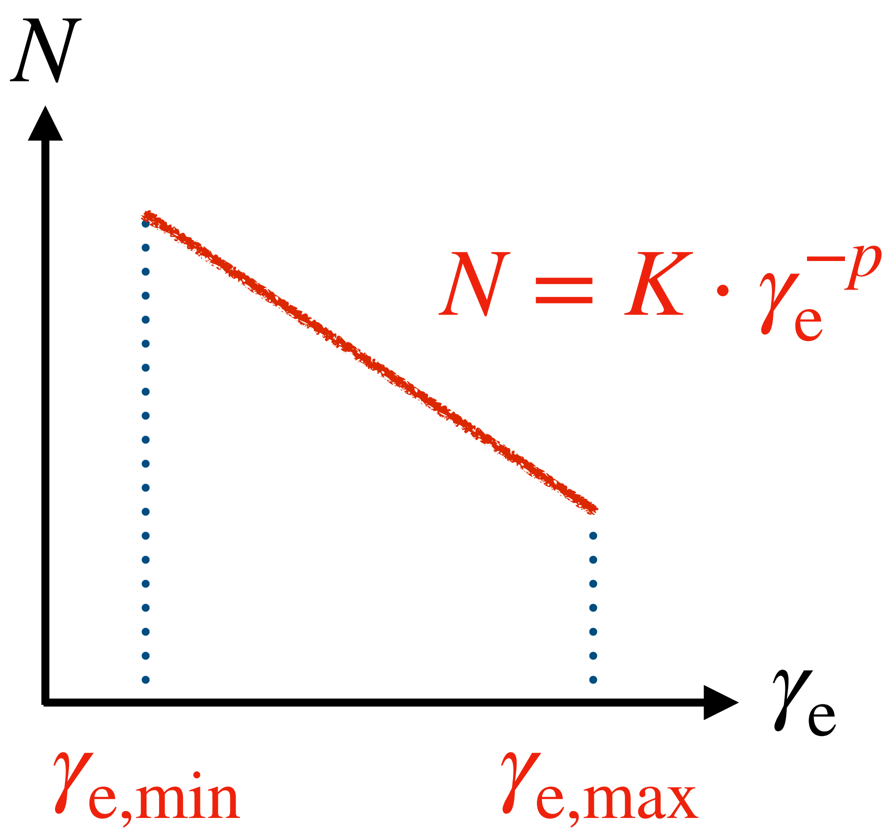

$$K = f(e_{\mathrm{th,e}}\,, C_{\mathrm{E}}\,, p\,, n_{\mathrm{e}}\,)$$

$$e_{\mathrm{th,e}} = 0.01 \cdot e_{\mathrm{th}}$$

$$n_{\mathrm{e}} = 0.01 \cdot n$$

$$C_{\mathrm{E}} = \gamma_{\mathrm{e,max}} / \gamma_{\mathrm{e,min}} = 10^3$$

→no radiative losses !

$$\begin{aligned} j_\nu &= \delta^2 \cdot j_{\nu'} \\ \alpha_\nu &= \delta^{-1} \cdot \alpha_{\nu'} \\ \tau_\nu &= \tau_{\nu'} \end{aligned}$$

$$\delta = \left(\gamma\left(1 - \beta \cdot \cos\left(\theta_{\mathrm{obs}}\right)\right)\right)^{-1}$$

POST PROCESSING :

- Injection following a power-law between two cut-off values;
- K depends on the density and thermal energy medium, as well as $\gamma_{\mathrm{e,min}}$ (Gomez et al. 1995).
- Our model takes into account Doppler relativistic effects with the observation angle θ_{obs}.

Magnetic field configuration

PUBLISHED IN A&A (FICHET DE CLAIRFONTAINE ET AL. 2021):

- General study on the impact of a magnetic field configuration :
  - ➡ **H**ydrodynamic : turbulent magnetic field;
  - ➡ **T**oroidal;
  - ➡ **P**oloidal;
  - ➡ **H**elical ($\theta_B = 45°$).

Low jet magnetization : $\sigma \leq 10^{-2}$, in order to allow diffusive acceleration on internal shocks.

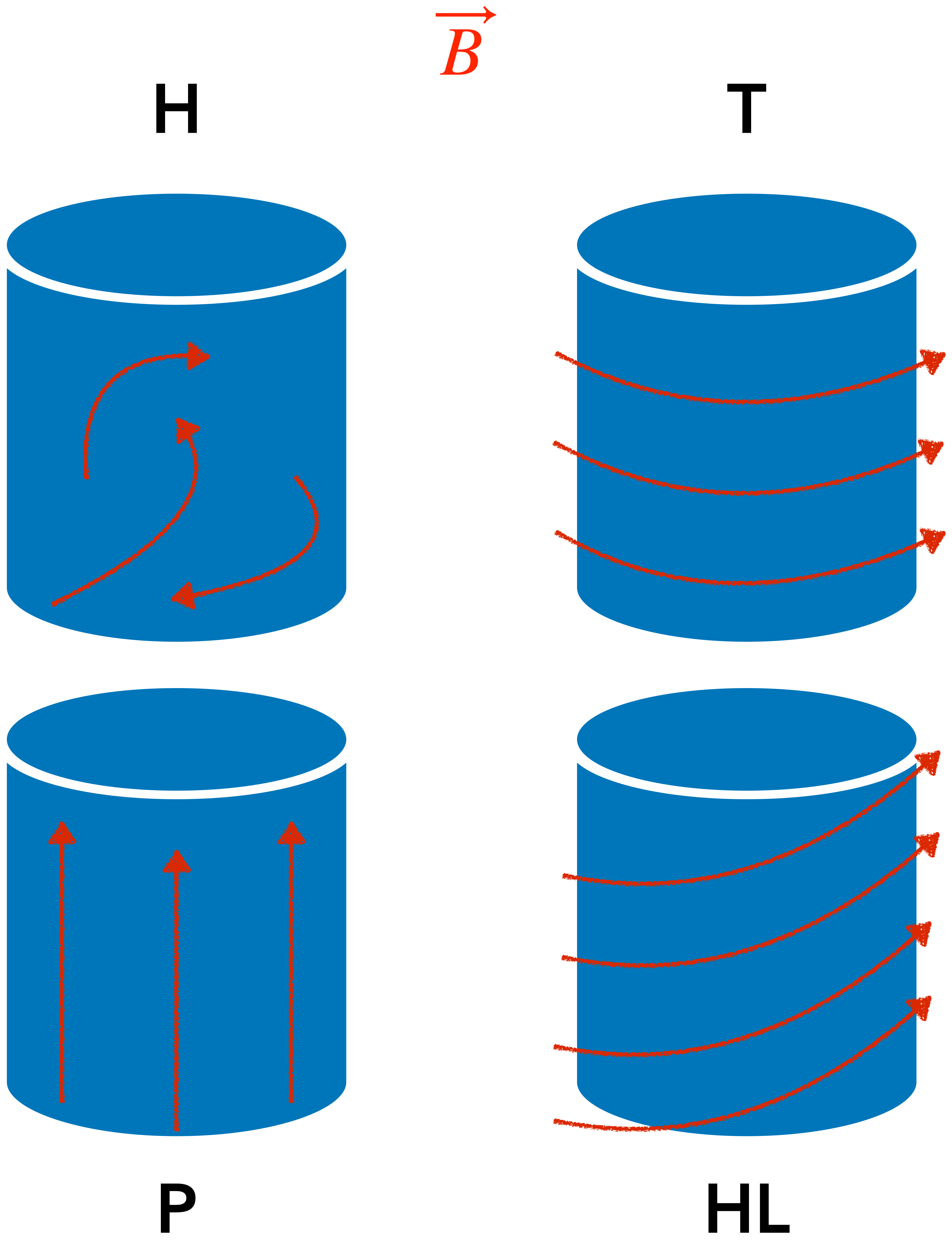

From SRMHD jet simulation to 2D map and light curve

Double component, toroidal case of jet

Thermal energy

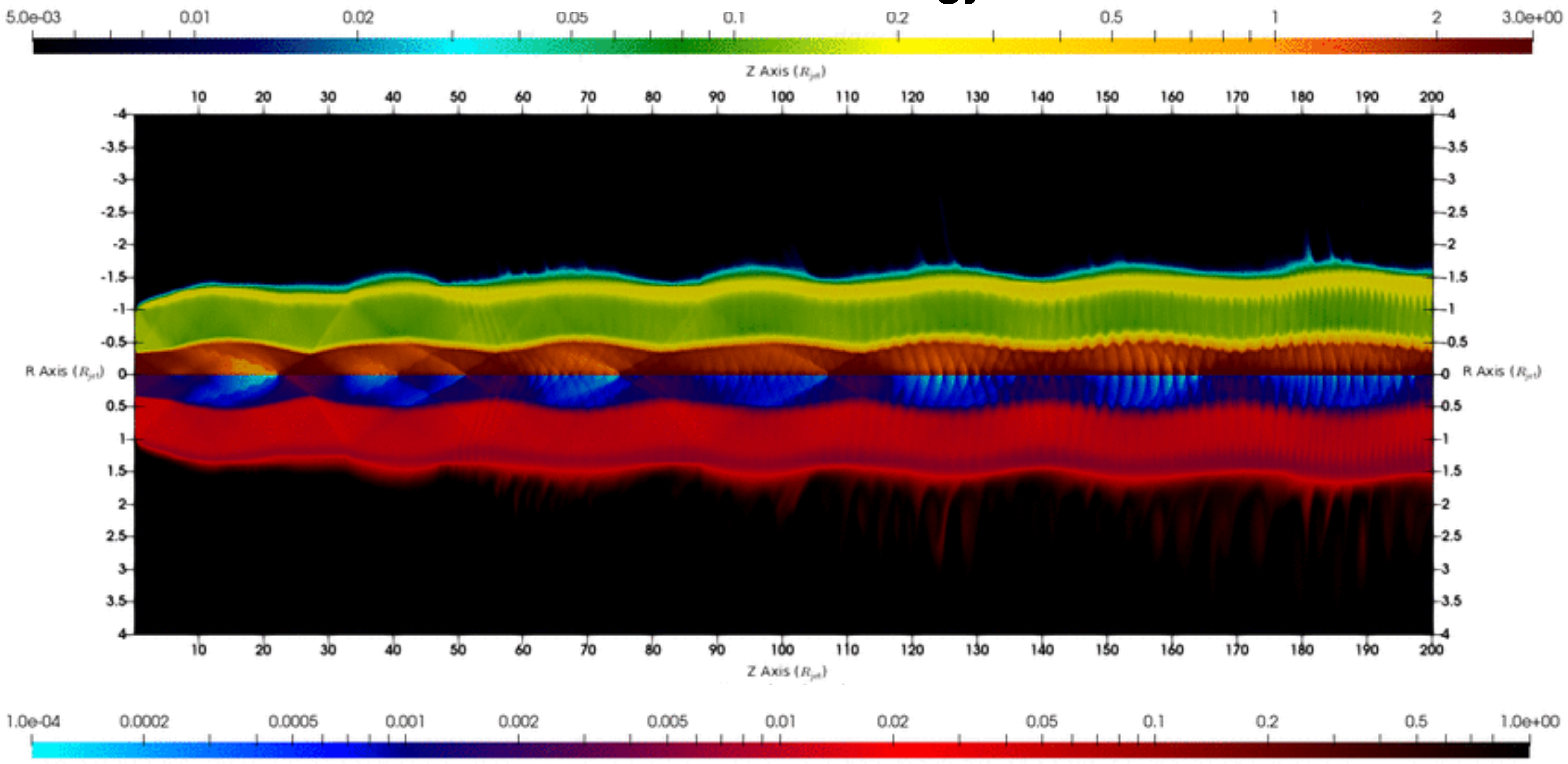

Density

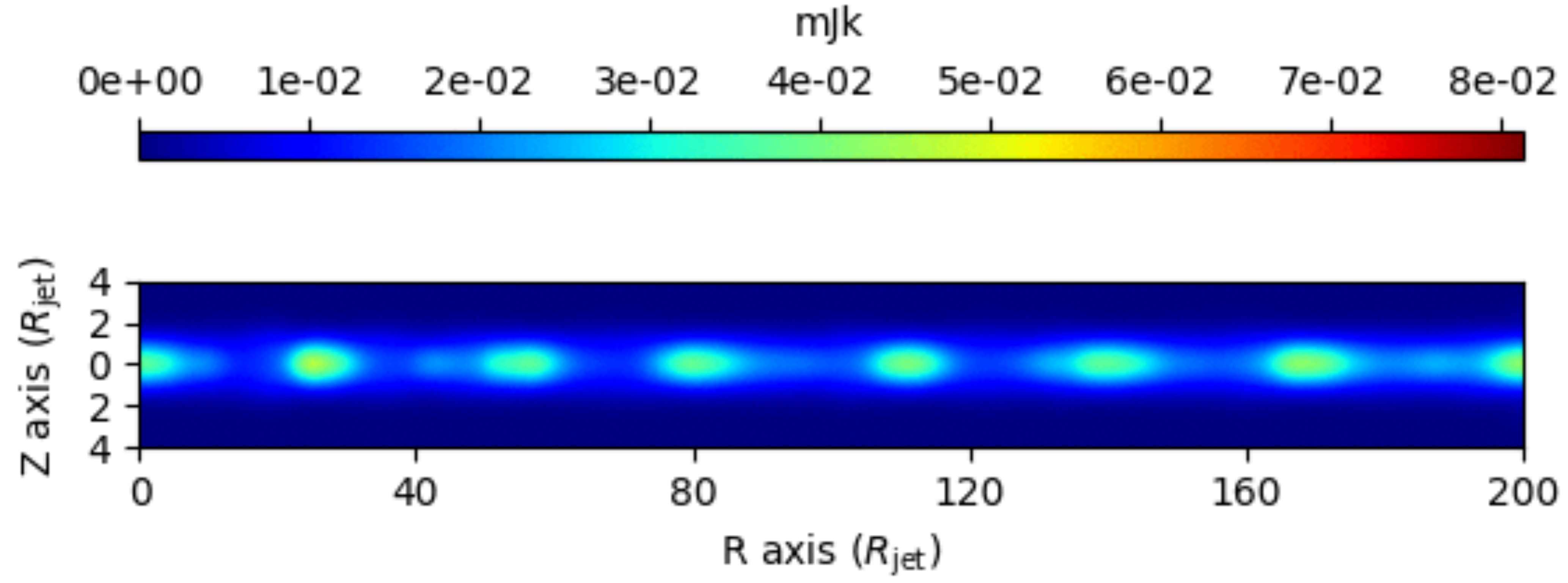

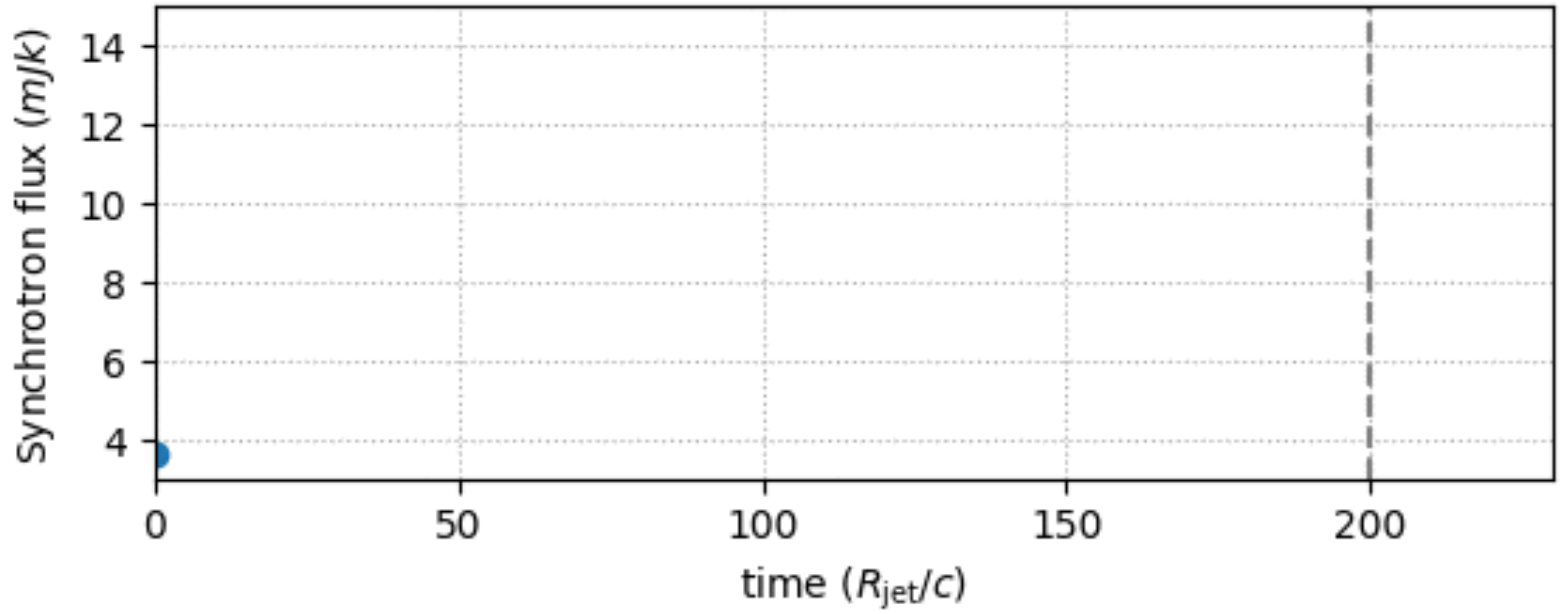

$\theta_{obs} = 90°$ and $\nu = 10^9$ Hz.

From SRMHD jet simulation to 2D map and light curve

Double component, toroidal case of jet

e_{th}

Thermal energy

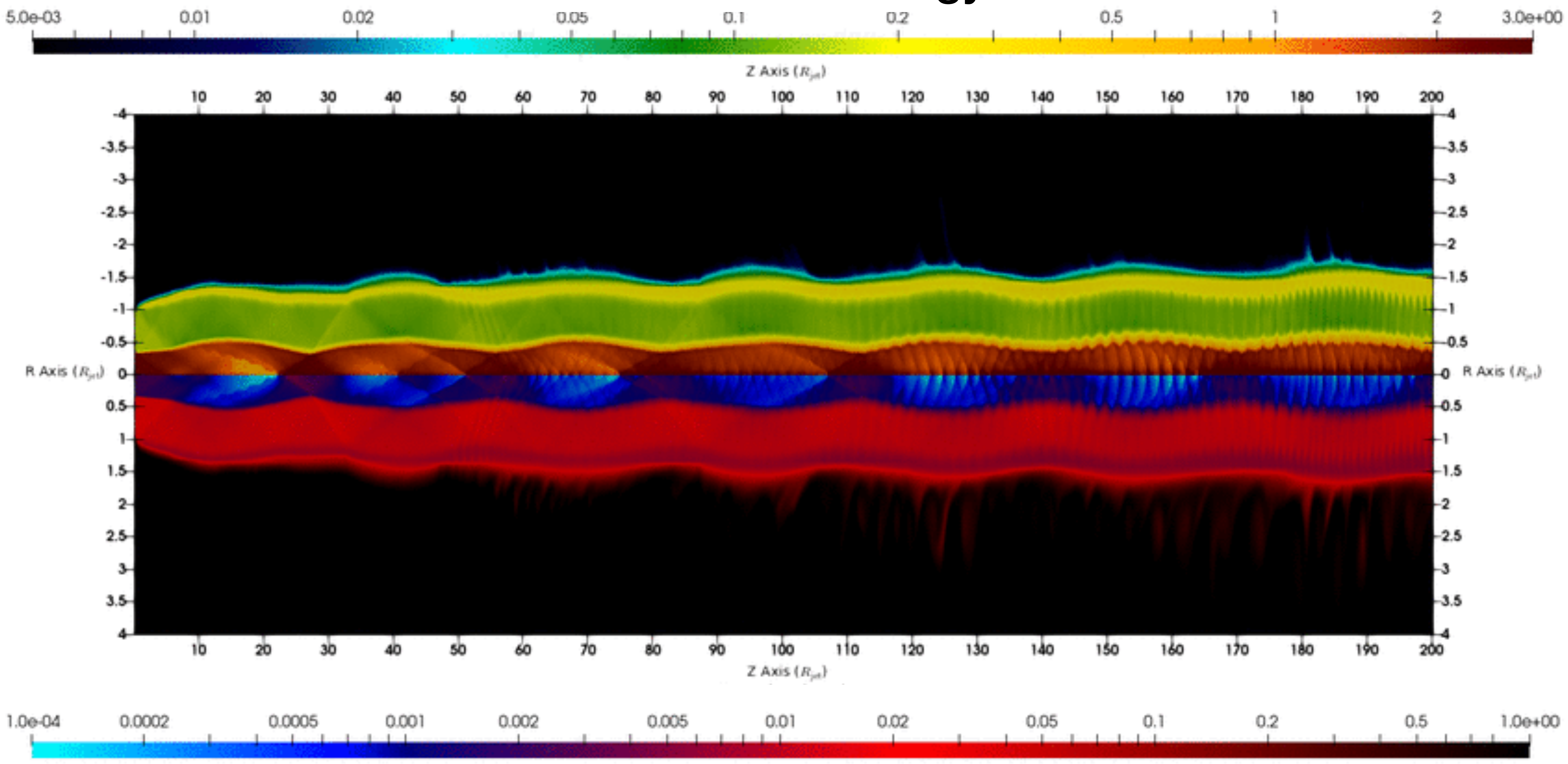

Density

$\sim n$

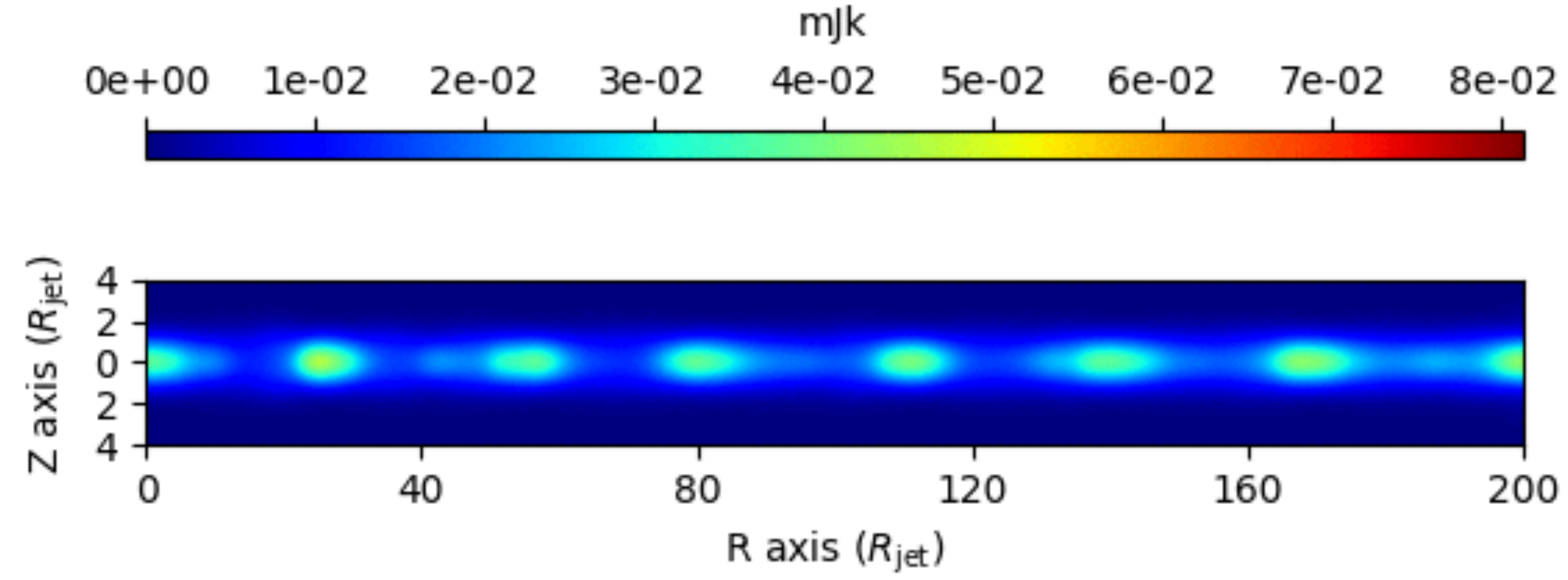

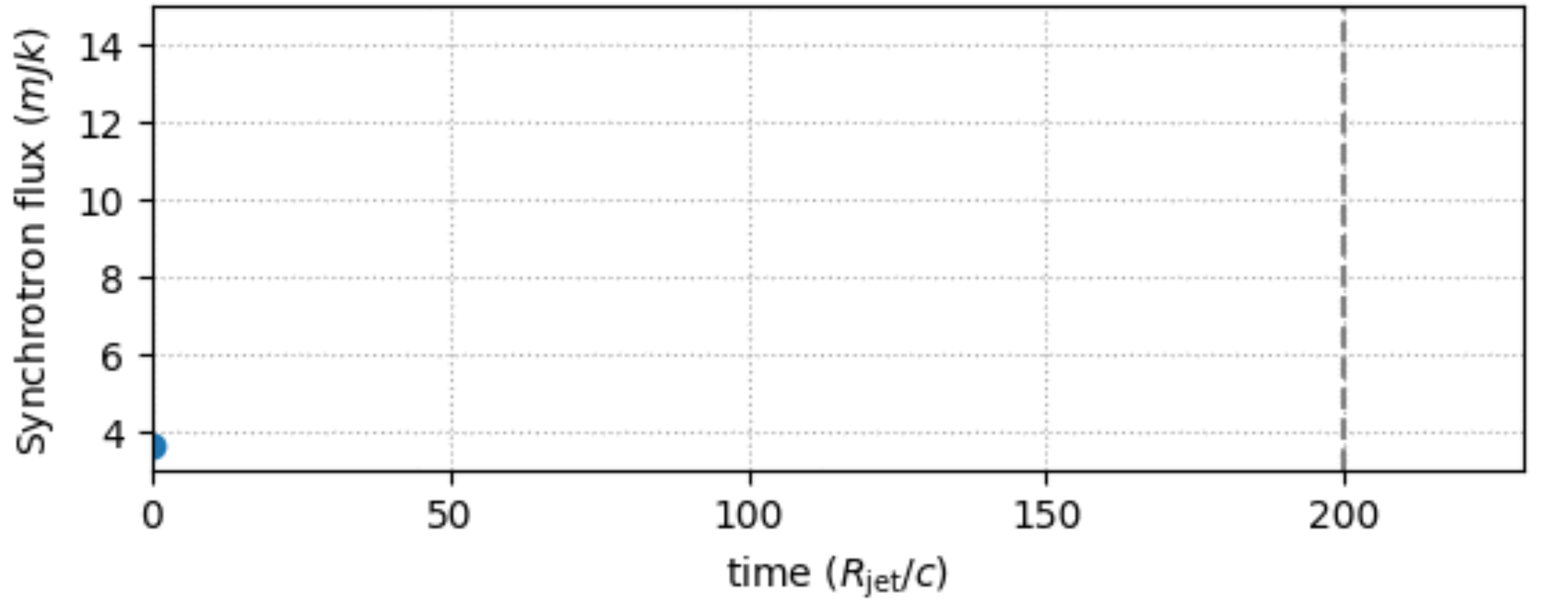

$\theta_{obs} = 90°$ and $\nu = 10^9$ Hz.

From SRMHD jet simulation to 2D map and light curve

Double component, toroidal case of jet

e_{th}

Thermal energy

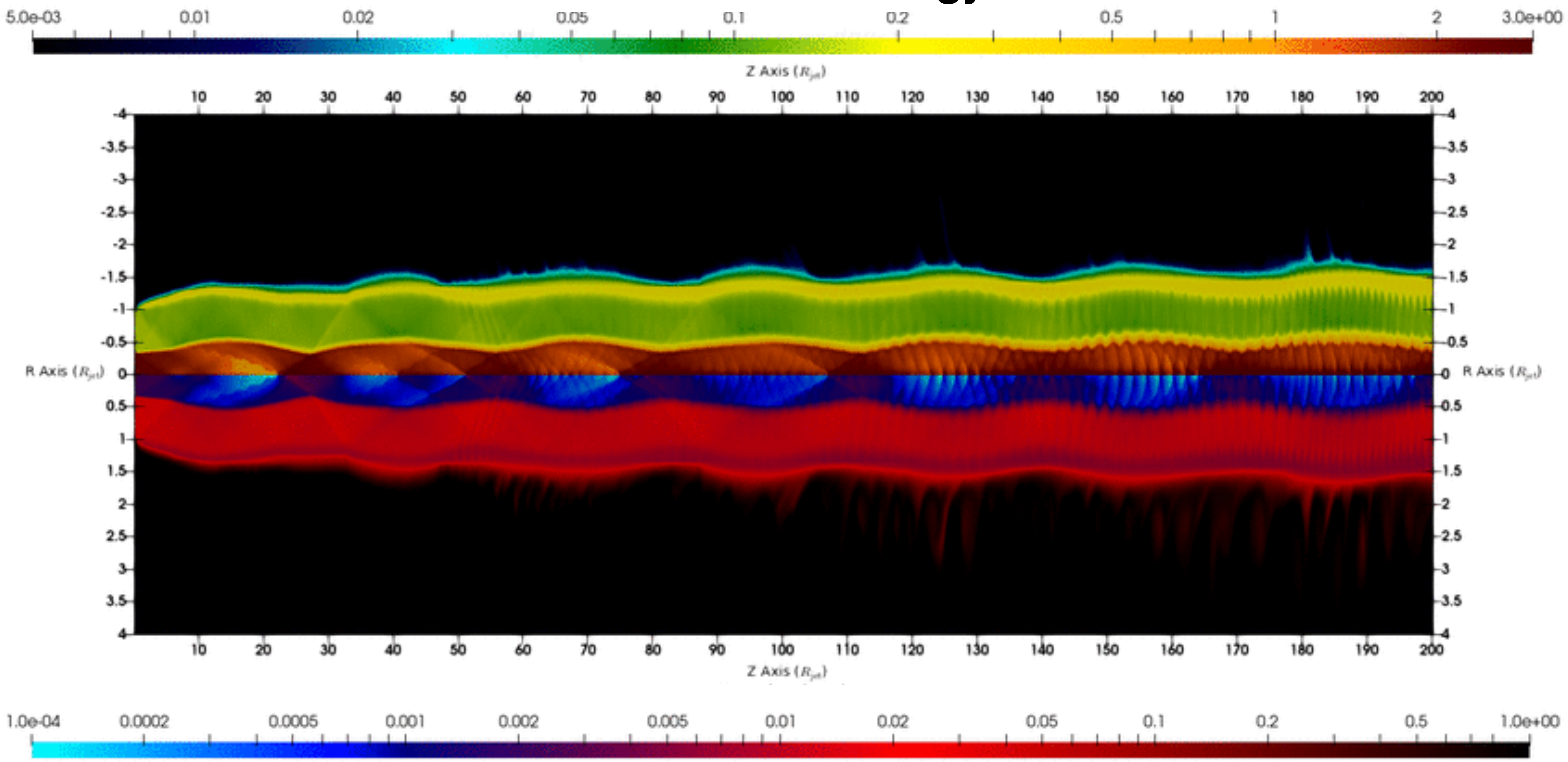

Density

$\sim n$

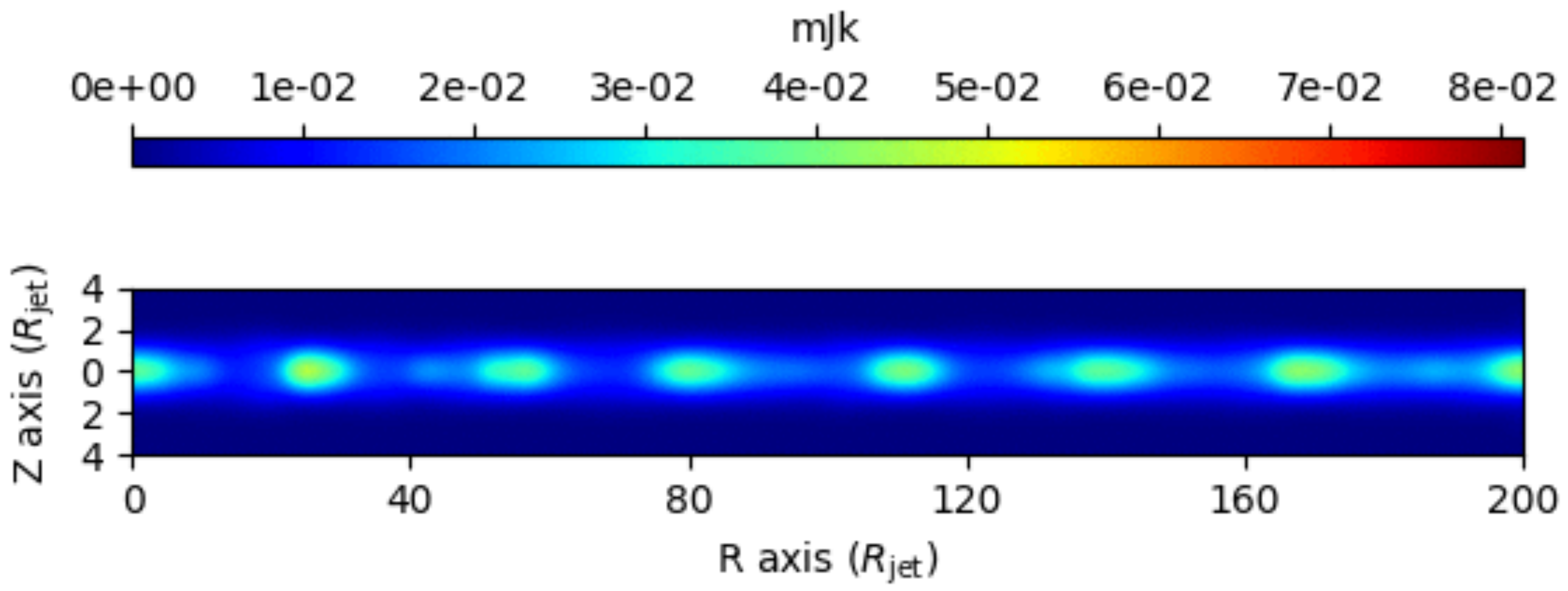

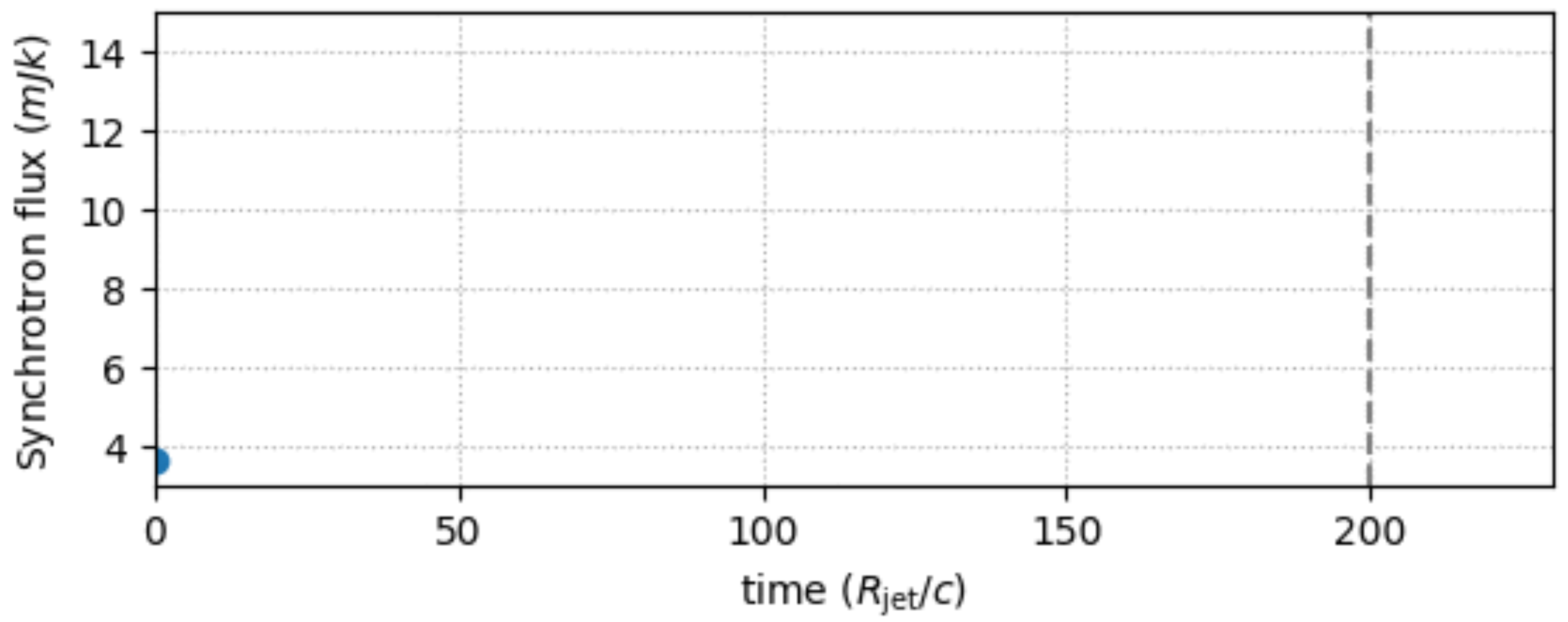

$\theta_{\rm obs} = 90°$ and $\nu = 10^9$ Hz.

From SRMHD jet simulation to 2D map and light curve

Double component, toroidal case of jet

e_{th}

Thermal energy

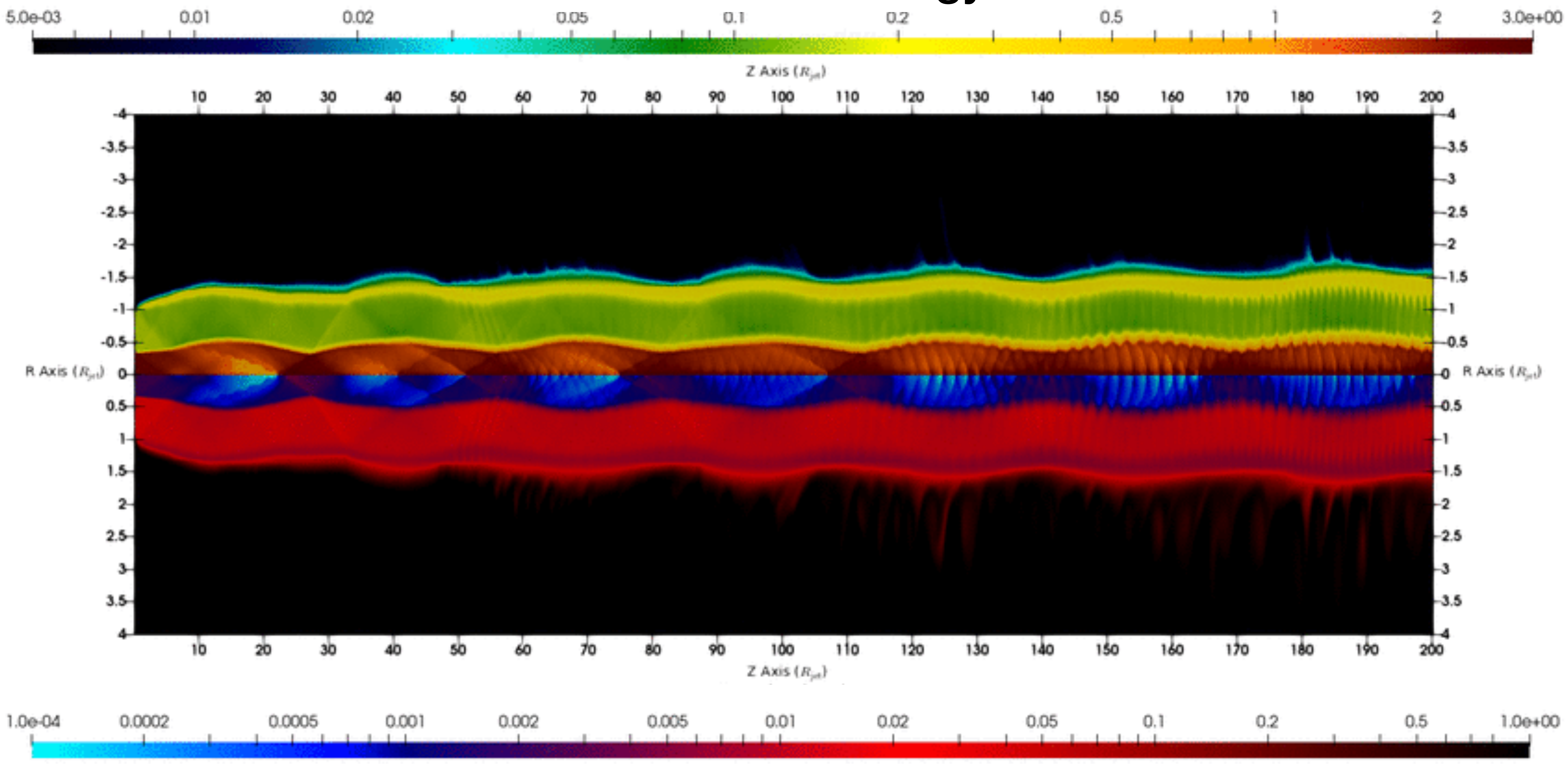

Density

$\sim n$

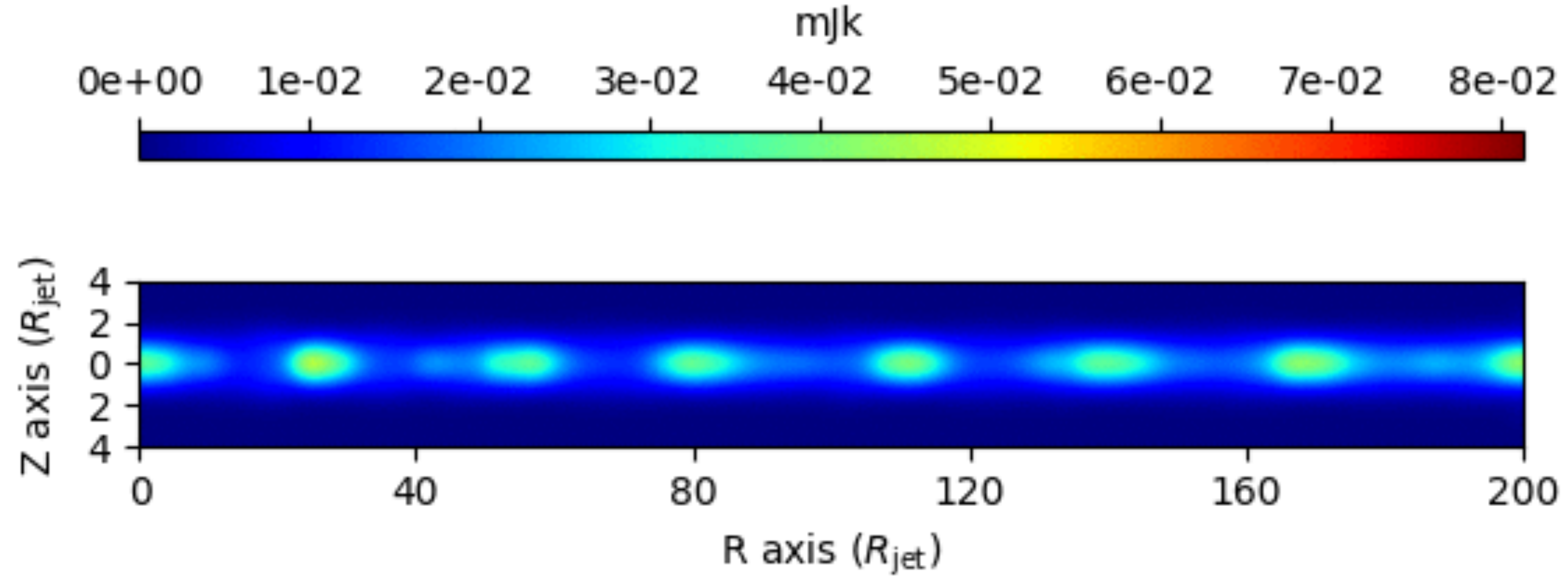

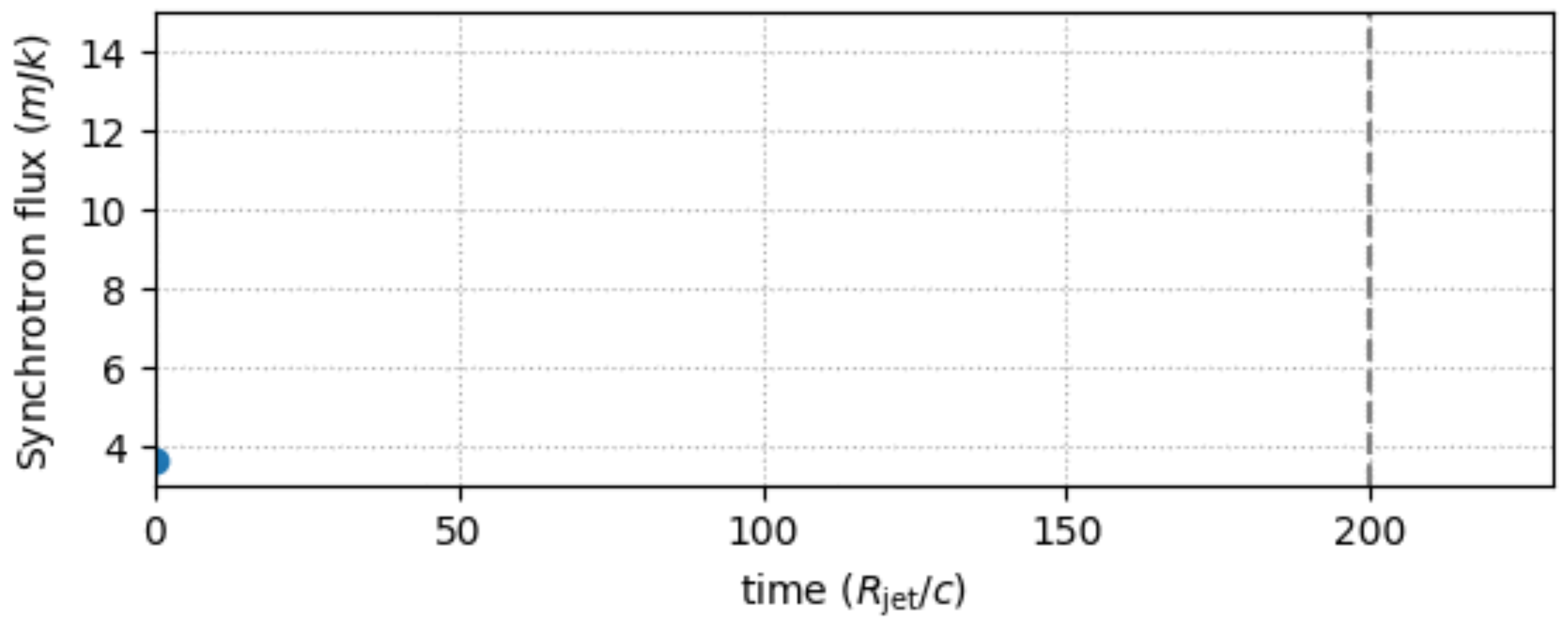

$\theta_{obs} = 90°$ and $\nu = 10^9$ Hz.

From SRMHD jet simulation to 2D map and light curve

Double component, toroidal case of jet

e_{th}

Thermal energy

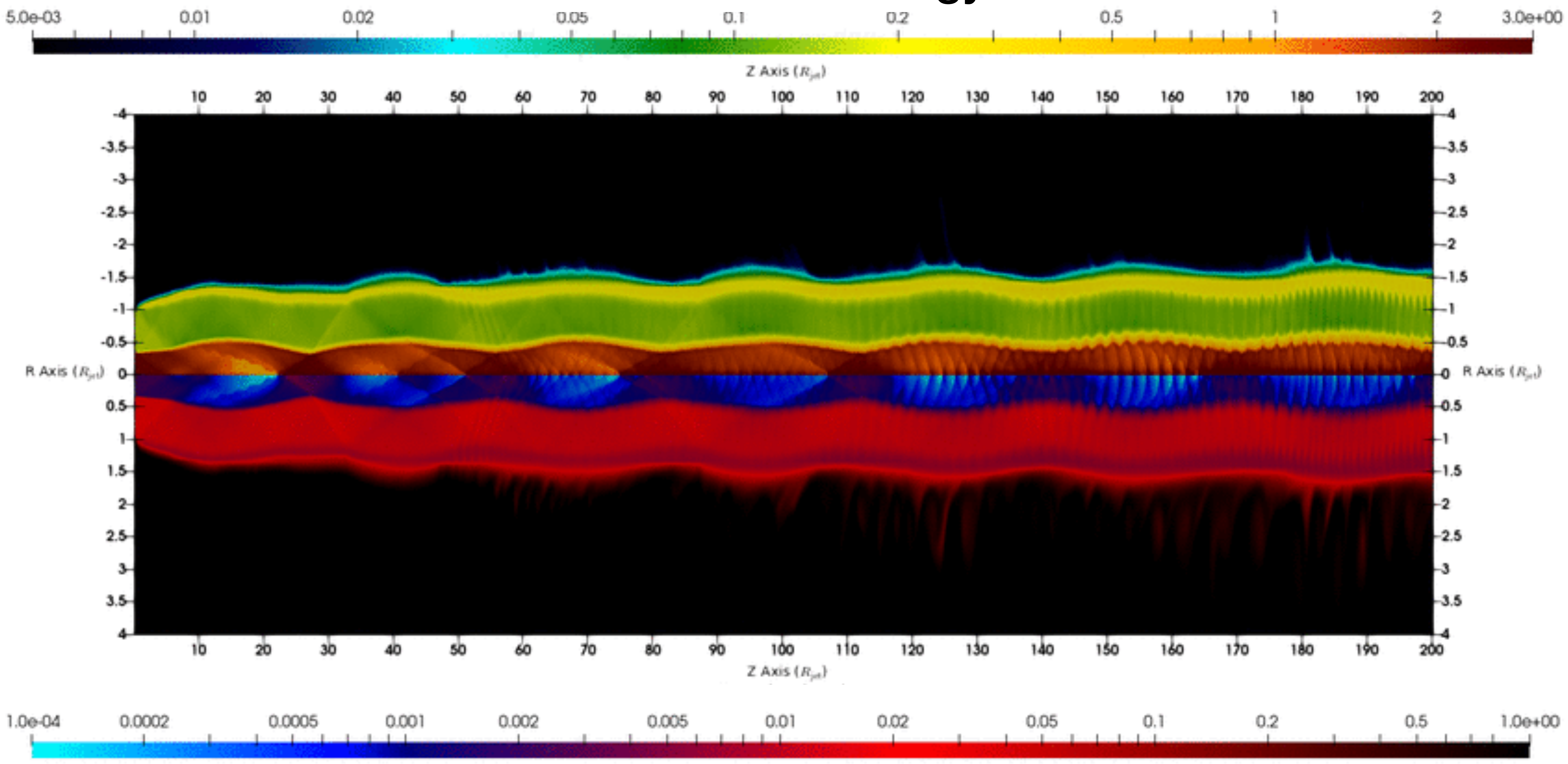

Density

$\sim n$

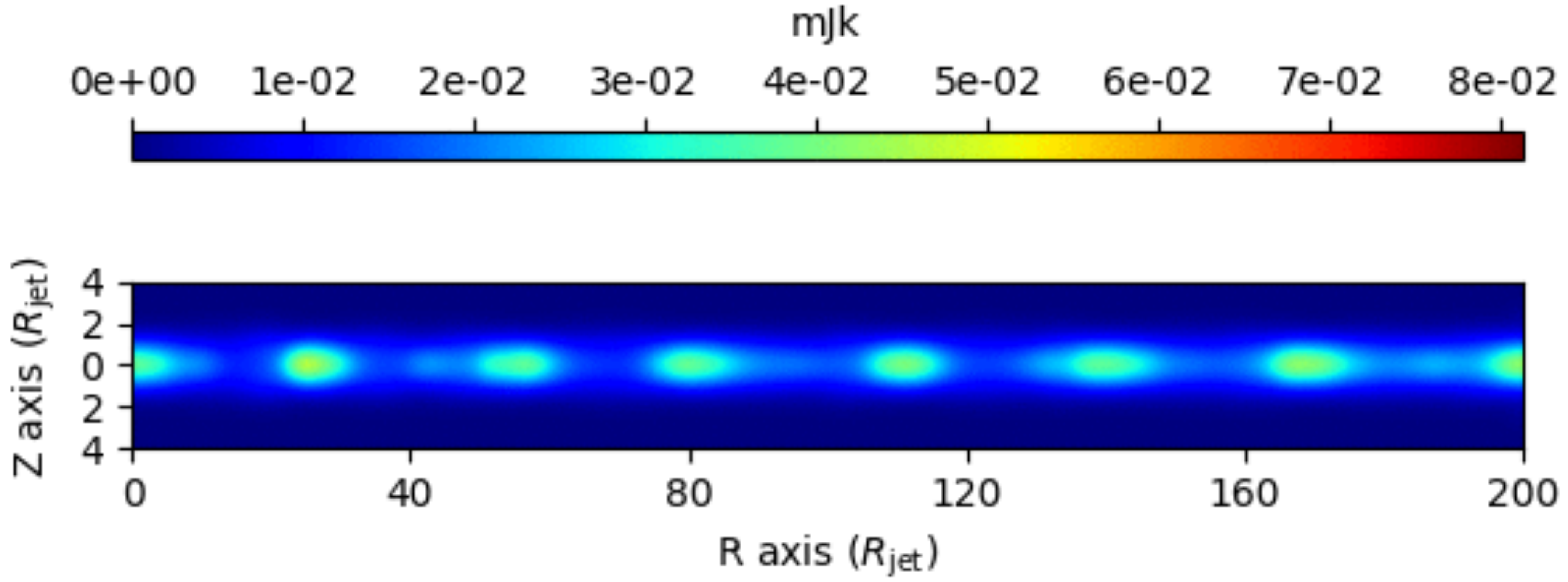

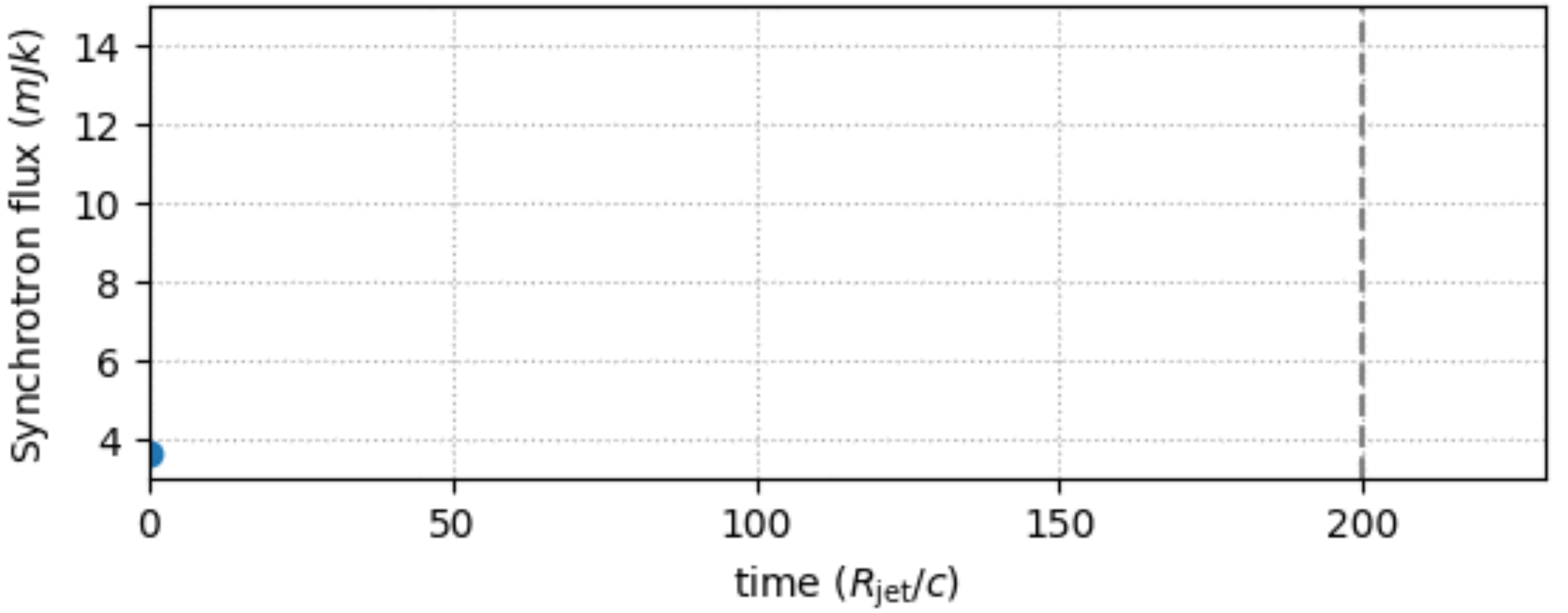

$\theta_{obs} = 90°$ and $\nu = 10^9$ Hz.

Light curves

Flux origin :

Ejecta — Jet — Total (Ejecta + Jet)

PUBLISHED IN A&A (FICHET DE CLAIRFONTAINE ET AL. 2021):

- Flare event during each moving / standing shock interaction;
- **H** / **T** : flux coming from the moving shock region, marked flares;
- **P** / **HL** : flux coming from the jet itself, less marked flares.

H : Hydrodynamic **P : Poloidal**

T : Toroidal **HL : Helical**

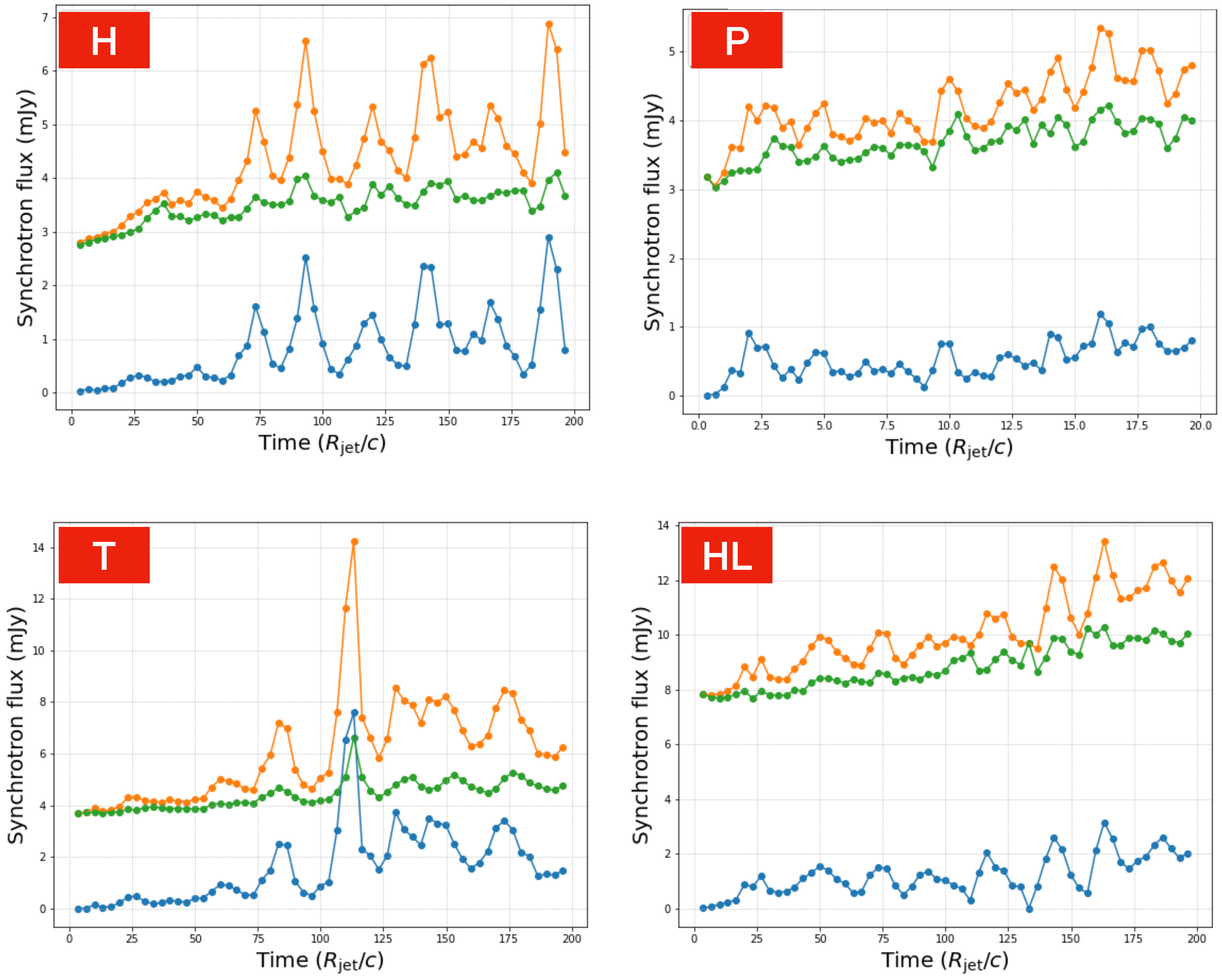

Four light curves for each case - $\theta_{\rm obs} = 90°$ and $\nu = 10^9$ Hz.

Application to 3C 273

PUBLISHED IN A&A (<u>FICHET DE CLAIRFONTAINE ET AL. 2021</u>):

- Qualitative comparison with radio flare event in 2014 in 3C 273;
- Observational constraints :
  - ✓ Observation frequency 15 GHz (OVRO Telescope);
  - ✓ Observation angle $\theta_{\text{obs}} = 2°$.
- From observations : flares during first moving / standing emission zone;
- <u>Flare asymmetry compatible.</u>

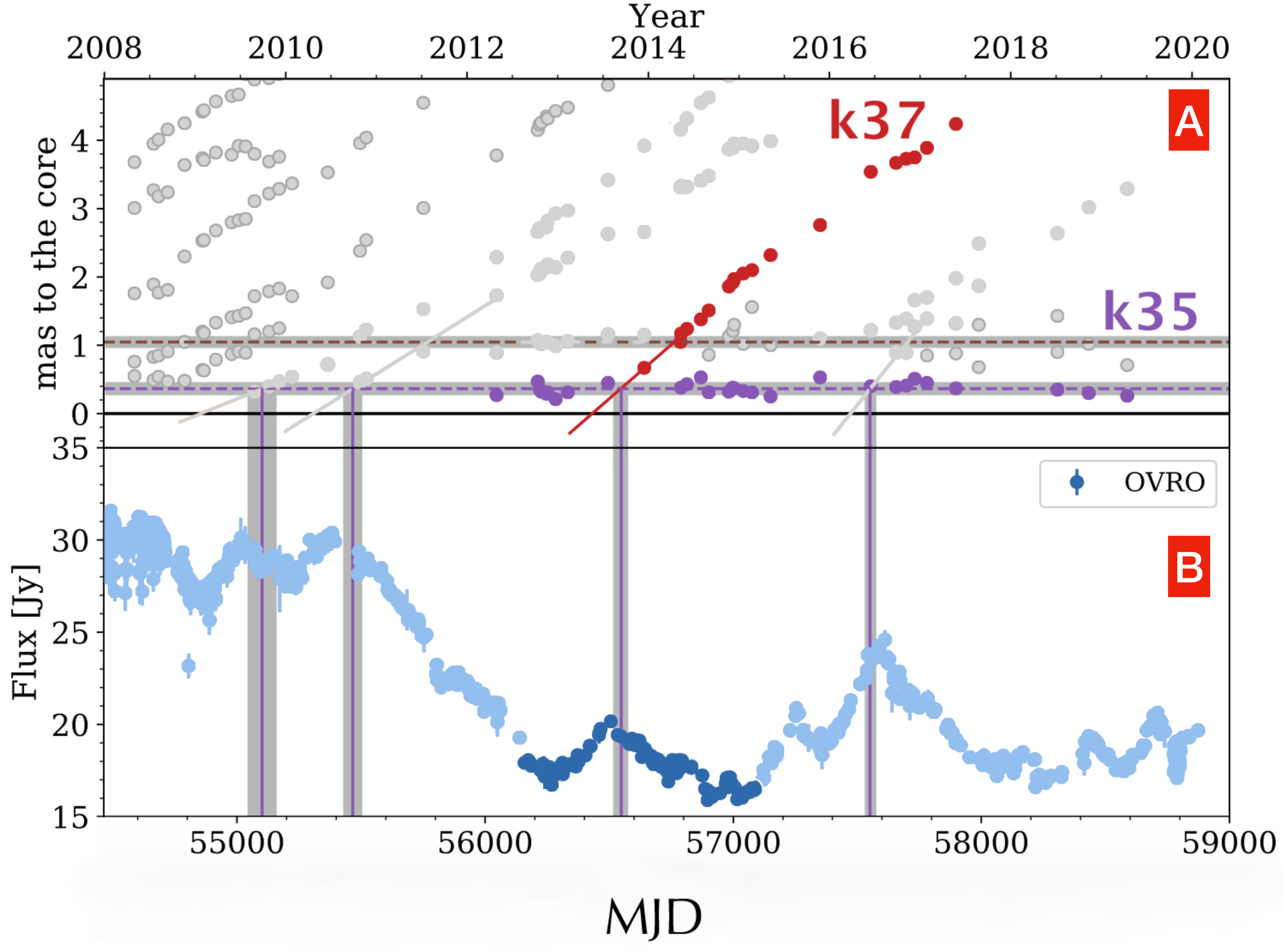

A : Distance to the core of radio knots analyzed by MOJAVE.
B : Radio jet light curve observed by OVRO.

Application to 3C 273

PUBLISHED IN A&A (FICHET DE CLAIRFONTAINE ET AL. 2021):

- Qualitative comparison with radio flare event in 2014 in 3C 273;
- Observational constraints :
  - ✓ Observation frequency 15 GHz (OVRO Telescope);
  - ✓ Observation angle $\theta_{\rm obs} = 2°$.
- From observations : flares during first moving / standing emission zone;
- Flare asymmetry compatible.

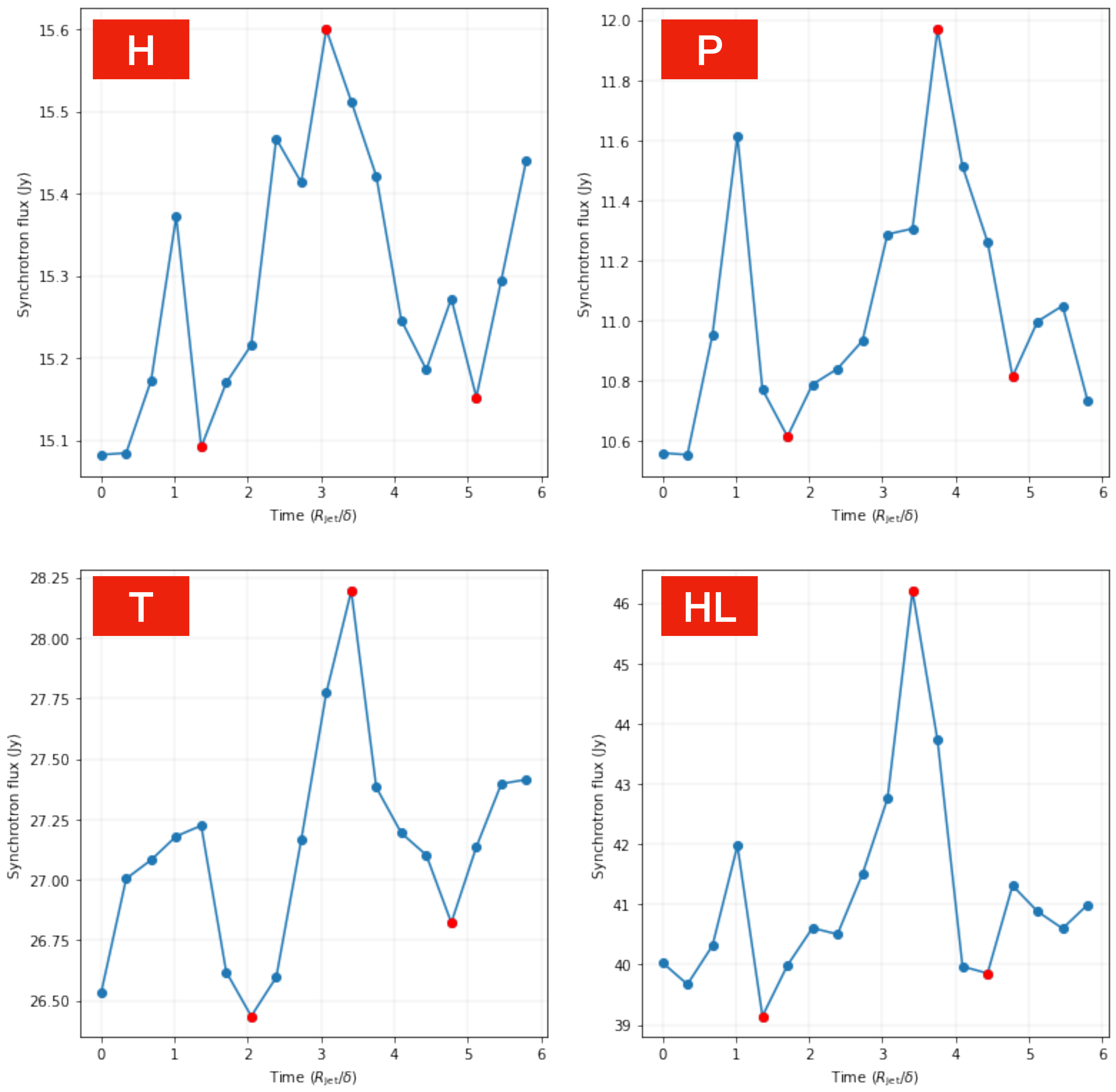

$\theta_{\rm obs} = 2°$ and $\nu = 15$ GHz.

Conclusion

WHAT HAS BEEN DONE :

✓ Clear dichotomy on the influence of toroidal / poloidal field;

✓ First comparison with observational characteristics looks promising.

PROSPECTS :

➡ <u>New effects added</u> : injection of electrons on detected shock (radiative cooling, time delay) during propagation of perturbation, flare relaxation (article in prep.);

➡ <u>Dedicated study on a specific object</u> : the goal is to reproduce observations from radio up to X band (jet morphology, variability, etc.).

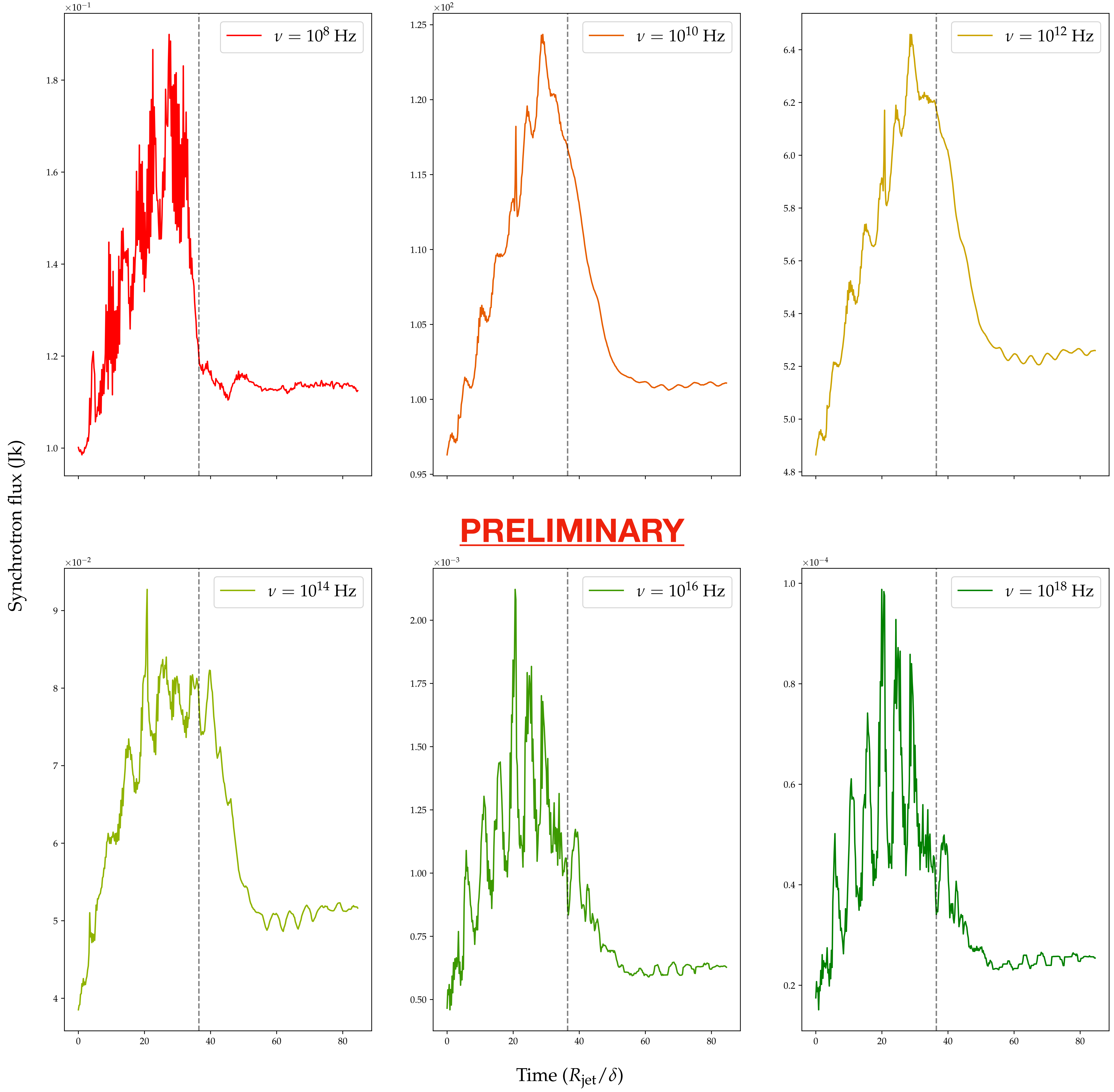

A GLIMPSE (G.FICHET DE CLAIRFONTAINE ET AL., IN PREP):

- Light curve obtained during the propagation of an ejecta inside a one-component magnetic-turbulent jet;
- Result obtained at different frequencies (from radio up to X band) and with $\theta_{\rm obs} = 10°$;
- Different variability obtained compatible with one observed;
- Emission coming from the moving shock and from jet relaxation.

Bonus : 2D synchrotron maps

ACCEPTED IN A&A (FICHET DE CLAIRFONTAINE ET AL. 2021):

- General study on the impact of a magnetic field configuration (four cases tested);
- Standing shock morphology : difference between H - T and P - HL :
  - Magnetic tension in T ⟶ compact;
  - Poloidal component ⟶ instabilities.

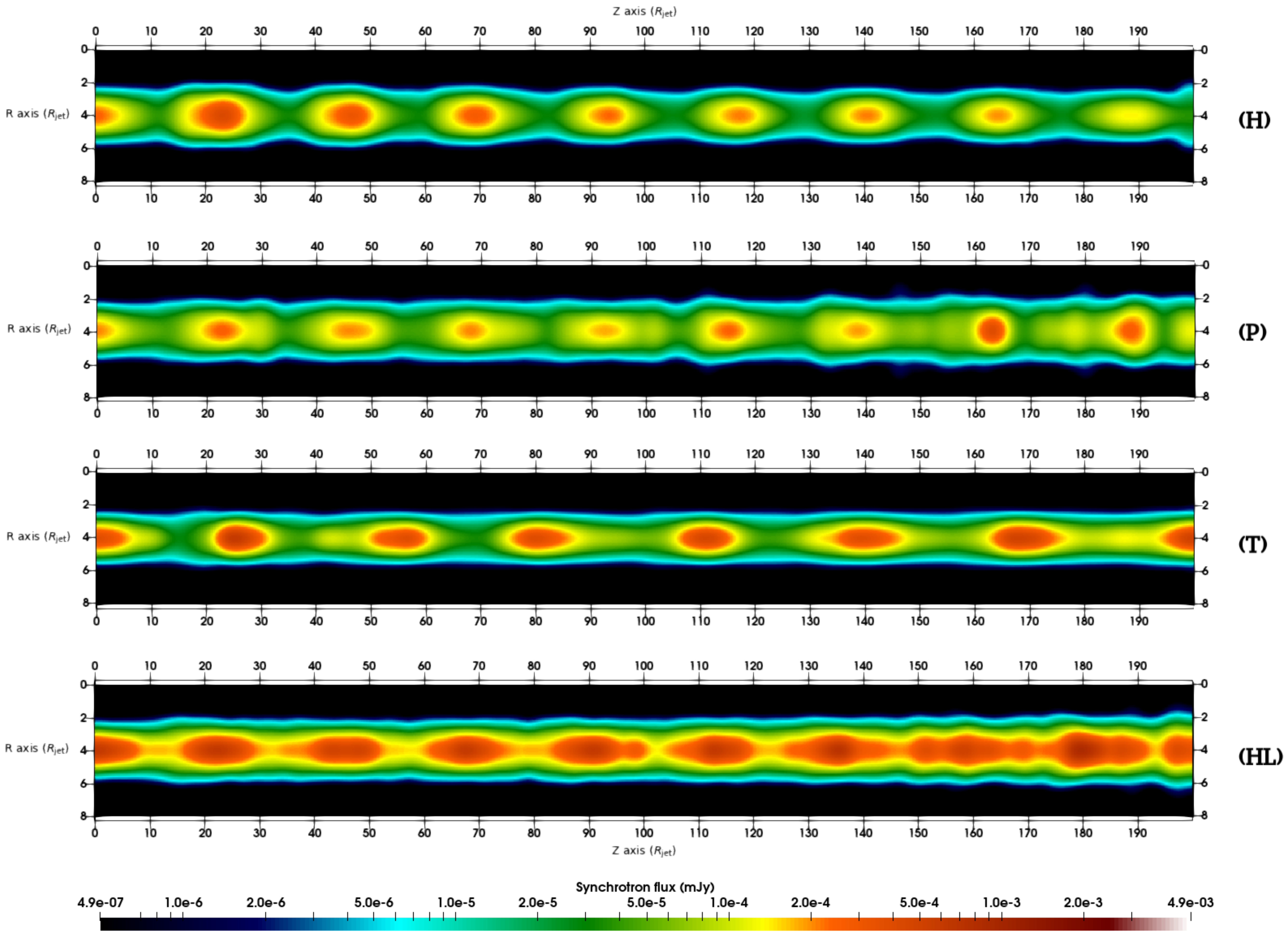

Bonus : 2D synchrotron maps

ACCEPTED IN A&A (FICHET DE CLAIRFONTAINE ET AL. 2021):

- General study on the impact of a magnetic field configuration (four cases tested);
- Standing shock morphology : difference between H - T and P - HL :
  - Magnetic tension in T ⟶ compact;
  - Poloidal component ⟶ instabilities.

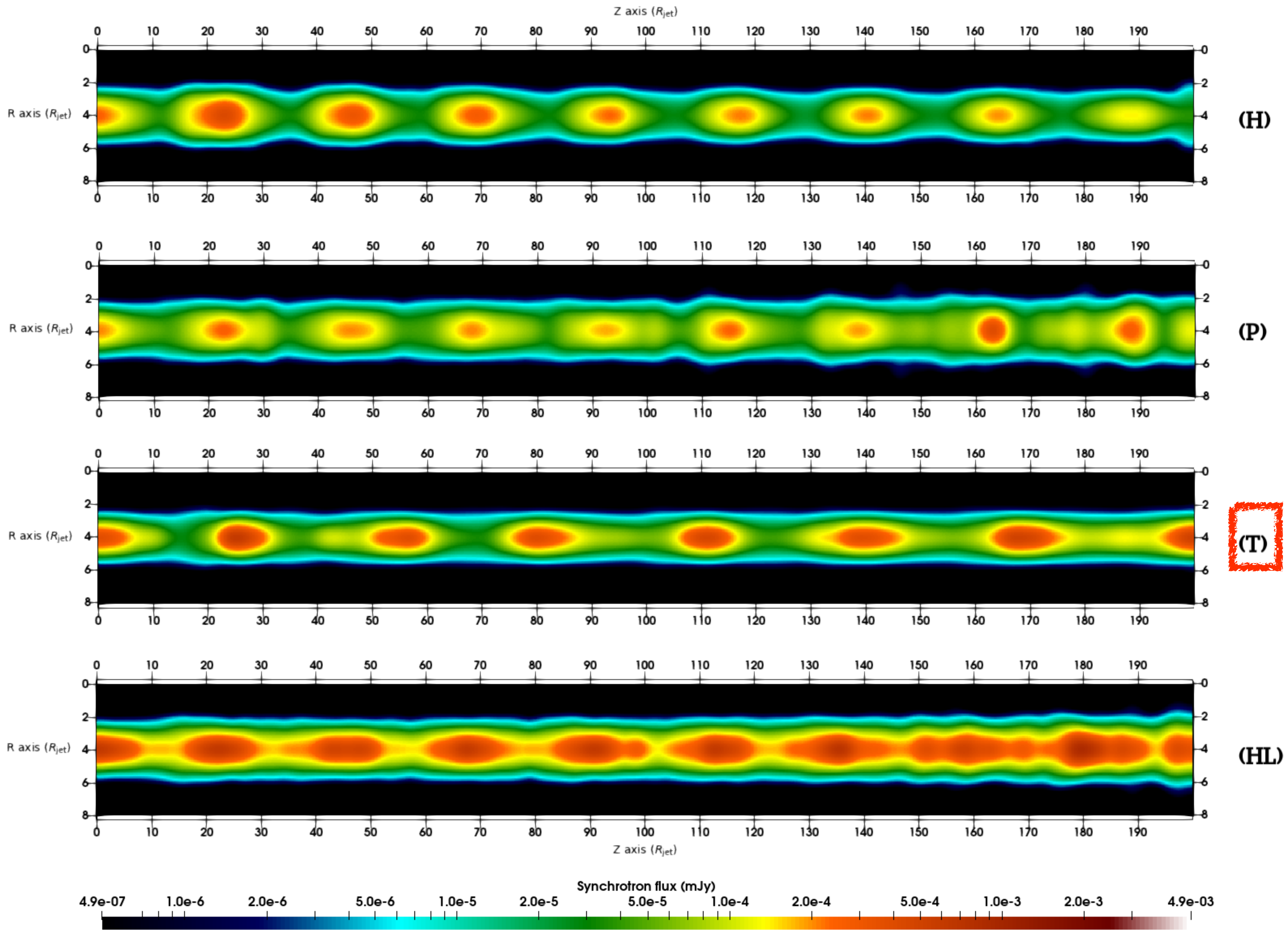

Bonus : 2D synchrotron maps

ACCEPTED IN A&A (FICHET DE CLAIRFONTAINE ET AL. 2021):

- General study on the impact of a magnetic field configuration (four cases tested);
- Standing shock morphology : difference between H - T and P - HL :
  - Magnetic tension in T ⟶ compact;
  - Poloidal component ⟶ instabilities.